The Second Derivative Electronic Absorption Spectrum of Cytochrome *c* Oxidase in the Soret Region

Martin P. Horvath, Robert A. Copeland, and Marvin W. Makinen
Department of Biochemistry and Molecular Biology, The University of Chicago, Cummings Life Science Center, Chicago, Illinois 60637 USA

ABSTRACT The electronic absorption spectrum of solubilized beef heart cytochrome *c* oxidase was analyzed in the 400–500 nm region to identify the origin of doublet features appearing in the second derivative spectrum associated with ferrocytochrome *a*. This doublet, centered near 22,600 cm^{-1}, was observed in the direct absorption spectrum of the $a^{2+}a_3^{3+}$·$HCOO^-$ form of the enzyme at cryogenic temperatures. Since evidence for this doublet at room temperature is obtained only on the basis of the second derivative spectrum, a novel mathematical approach was developed to analyze the resolving power of second derivative spectroscopy as a function of parameterization of spectral data. Within the mathematical limits defined for resolving spectral features, it was demonstrated that the integrated intensity of the doublet feature near 450 nm associated with ferrocytochrome *a* is independent of the ligand and oxidation state of cytochrome a_3. Furthermore, the doublet features, also observed in cytochrome *c* oxidase from *Paracoccus denitrificans*, were similarly associated with the heme *A* component and were correspondingly independent of the ligand and oxidation state of the heme A_3 chromophore. The doublet features are attributed to lifting of the degeneracy of the *x* and *y* polarized components of the B state of the heme *A* chromophore associated with the Soret transition.

INTRODUCTION

Cytochrome *c* oxidase (EC 1.9.3.1) is the terminal enzyme of the electron transport chain in mitochondria and bacteria, catalyzing the oxidation of cytochrome *c* and reduction of molecular dioxygen to water. This thermodynamically favorable process is coupled to the energetically unfavorable translocation of protons across the inner mitochondrial membrane (Wikström, 1977; Wikström and Krab, 1979; Saraste, 1990). Understanding the mechanisms by which enzymes couple unfavorable and favorable transport and chemical processes is of central importance in biochemistry. A fundamental requirement for coupling of two such reactions is that they are linked by a common structural intermediate of the enzyme (DeVault, 1971; DeVault, 1976; Jencks, 1980; Tanford, 1983). According to this model, protein structural rearrangements occur in the favorable chemical reaction, and a portion of the free energy from the chemical reaction is stored in the conformational state of the protein. In the unfavorable process, the enzyme returns to its ground-state conformation, whereby the ensuing change in free energy drives the unfavorable transport reaction.

In cytochrome *c* oxidase, there are two heme *A* prosthetic groups and two copper centers that participate in electron transfer and dioxygen reduction (Vanneste, 1966; Antholine et al., 1992; Babcock and Wikström, 1992; Blackburn et al., 1994; van Wachenfeldt et al., 1994; Tsukihara et al., 1995). Since the electronic structure of the heme prosthetic groups may be sensitive to perturbations from the protein, conformational states involved in coupling electron transfer and proton translocation may be distinguishable by electronic absorption spectroscopy. Because there is extensive overlap in the spectra of the heme *A* and heme A_3 groups (Vanneste, 1966), second derivative absorption spectroscopy (Williams and Hager, 1970; Cahill, 1979) has been applied to cytochrome *c* oxidase to separate their characteristic features (Copeland, 1991, 1993; Ishibe et al., 1991; Sherman et al., 1991; Lynch et al., 1992; Felsch et al., 1994). The initial report of second derivative absorption spectra of cytochrome *c* oxidase showed a feature at 450 nm for ligand-bound forms of the enzyme that was not resolved in spectra of unliganded (reduced) cytochrome *c* oxidase, while the unliganded enzyme was associated with a feature at 440 nm (Sherman et al., 1991). The feature at 450 nm was assigned to cytochrome *a* in the Fe^{2+} oxidation state by comparing the spectra of the mixed-valence $a^{3+}a_3^{2+}$·CO form* of the mammalian enzyme with that of the fully reduced $a^{2+}a_3^{2+}$·CO form (Sherman et al., 1991) or by comparing second derivative absorption spectra of bacterial forms of cytochrome *c* oxidases with naturally occurring porphyrin cofactor substitutions (Felsch et al., 1994). Because ligand

Received for publication 25 January 1999 and in final form 20 May 1999.

Address reprint requests to Dr. Marvin W. Makinen, Department of Biochemistry and Molecular Biology, The University of Chicago, 920 East 58th Street, Chicago, IL 60637. Tel.: 773-702-1080; Fax: 773-702-0439; E-mail: m-makinen@uchicago.edu.

Dr. Horvath's present address is Department of Chemistry and Biochemistry, University of Colorado, Boulder, CO 80309.

Dr. Copeland's present address is Department of Chemical Enzymology, The DuPont Pharmaceuticals Company, P.O. Box 80400, Wilmington, DE 19880-0400.

Abbreviations used: HEPES, 4-(2-hydroxyethyl)-1-piperazineethanesulfonic acid; EDTA, ethylene-diaminetetraacetic acid; TMPD, *N*,*N*,*N*′,*N*′-tetramethyl-*p*-phenylenediamine.

0006-3495/99/09/1694/18 $2.00

*We refer to Fe(III) and Fe(II) states of the heme *A* and heme A_3 prosthetic groups in cytochrome *c* oxidase as $a^{3+}a_3^{3+}$, viz. $a^{2+}a_3^{2+}$, etc. throughout.

binding at cytochrome a_3 appeared to be necessary to detect the 450-nm feature, it was suggested that ligand binding at cytochrome a_3 stabilized a conformation of the enzyme that was distinct from the conformation populated in the absence of ligand (Sherman et al., 1991). This conclusion stands in contradiction to results of studies in which cytochrome *a*:cytochrome a_3 interactions were evaluated on the basis of electronic absorption (Blair et al., 1982) or magnetic circular dichroism spectroscopy (Babcock et al., 1976). In these latter studies no differences in the electronic absorption spectra or magnetic circular dichroism spectra of cytochrome *a* were identified with changes in the ligand, oxidation, or spin state of cytochrome a_3.

In the present report, the two-component nature of the electronic absorption spectrum of cytochrome *a* at 450 nm is identified both on the basis of the direct absorption spectrum at cryogenic temperatures and through mathematical analysis of the resolving power of second derivative spectroscopy. We develop a method of quantitative analysis of absorption and second derivative absorption spectra of cytochrome *a* as a function of temperature and ligand and oxidation state of the enzyme complex. We show that the absorption feature at 450 nm derives from the excited state properties of the heme *A* chromophore and is not influenced by changes in ligand or oxidation state of the heme A_3 chromophore. The second derivative methodology developed here provides a sensitive means to evaluate changes in ligand and oxidation states of cytochrome *c* oxidase so that the overlapping contributions of the heme *A* and heme A_3 prosthetic groups can be separated from each other. The method is shown to be mathematically rigorous with respect to instrumentational details of data collection. Furthermore, the approach is general and can be adapted to other multicomponent systems with overlapping spectral features.

EXPERIMENTAL PROCEDURES

Materials

Purification of mitochondrial cytochrome c *oxidase*

Beef heart cytochrome *c* oxidase was purified by the method first described by Hartzell and Beinert (Hartzell and Beinert, 1974; Hartzell et al., 1978). The final ammonium sulfate precipitate was solubilized in a solution containing 1% (w/w) lauryl-β-D-maltoside (Anatrace, Maumee, OH) buffered with 0.05 M HEPES at pH 7.4. After overnight dialysis, the enzyme was concentrated to greater than 500 μM in cytochrome *c* oxidase with the use of a Centriprep-30 device (Amicon, Beverly, MA). The concentrated enzyme preparation was rapidly frozen in 100-μL aliquots in cryovials (Nunc, Naperville, IL) and stored at -80°C. The enzyme exhibited a maximal turnover rate for oxidation of horse heart ferrocytochrome *c* of 500 ± 40 s^{-1} at 25°C and a K_m of 17 ± 3 μM.

Purification of cytochrome c oxidase from Paracoccus denitrificans

Frozen cell paste harvested from large volume cultures of *P. denitrificans* grown under conditions of high oxygen tension was purchased from Philip Johnson at the Pilot Plant, Department of Biochemistry, University of Wisconsin, Madison, WI. Frozen cell paste (500 g) was submerged in buffer containing 0.1 M potassium phosphate at pH 7.6 and allowed to thaw. The combined volume of buffer and frozen cells was 1.4 L. The thawed cells were treated with 0.4 g hen egg white lysozyme (Sigma Chemical Co., St. Louis, MO), 0.02 M Mg^{2+} (either $MgCl_2$ or $MgSO_4$), and 1000 Kuntz units of DNAse (Sigma) for 30 min at room temperature with manual stirring. All subsequent operations were carried out on ice or at 4°C. The spheroplast preparation was sonicated at 40 W for 4 min and then centrifuged at $4000 \times g$ for 60 min. The cloudy, brown supernatant was carefully collected with the use of a siphon. The soft and stringy pellet was extracted with two volumes of ice-cold distilled water and the second supernatant was combined with the first. The bacterial membranes were collected by centrifugation at $20{,}000 \times g$ for 90 min and resuspended in 0.1 M potassium phosphate buffer at pH 7.6. This spheroplast preparation was rapidly frozen in 50 mL aliquots and stored at -80°C.

The spheroplasts prepared from 500 g of frozen cell paste were thawed on ice and then extracted by adding lauryl-β-D-maltoside to a final concentration of 0.5 g/g protein. Before addition, the solid detergent was dissolved in a small amount of distilled water. The extract was homogenized with a ground glass homogenizer, sonicated at 40 W for four 30-s intervals with the power off for 1 min between intervals, and then stirred at 4°C for 60 min. Solid sodium chloride was added to a final concentration of 0.18 M, and the extract was centrifuged at $35{,}000 \times g$ for 20 min. The supernatant was loaded onto a 200-mL Q-Sepharose FF (Pharmacia Biotech, Piscataway, NJ) column that had been previously equilibrated with 0.05 M Tris-HCl buffer at pH 7.8, containing 0.2 g/L lauryl-β-D-maltoside (chromatography buffer) and 0.1 M sodium chloride. The protein was applied to the column at a flow rate of 0.8 mL/min. Contaminating proteins were washed off of the column with 300 mL of chromatography buffer containing 0.25 M sodium chloride at a flow rate of 0.8 mL/min followed by 200 mL of chromatography buffer containing 0.35 M sodium chloride at a flow rate of 0.6 mL/min. The column was eluted with an 800-mL linear concentration gradient starting with chromatography buffer containing 0.35 M sodium chloride and ending with buffer containing 0.45 M sodium chloride followed by an additional 200 mL of buffer containing 0.45 M sodium chloride. The flow rate for the gradient elution and subsequent wash was 0.6 mL/min. Fractions containing cytochrome *c* oxidase were pooled and concentrated under nitrogen pressure to a volume of 50 mL over an Amicon YM-30 or PM-30 membrane.

The ionic strength of the Q-Sepharose purified material was adjusted by diluting the concentrated, pooled fractions eightfold to a final volume of 400 mL with chromatography buffer. The low ionic strength solution of Q-Sepharose purified cytochrome *c* oxidase was applied at a flow rate of 0.6 mL/min to a 30-mL horse heart cytochrome *c* affinity (Sigma) column that had been previously equilibrated with chromatography buffer containing 0.05 M potassium chloride. After loading the material, the column was washed at a flow rate of 0.3 mL/min with 150 mL chromatography buffer containing 0.05 M potassium chloride. Cytochrome *c* oxidase was eluted at a flow rate of 0.3 mL/min with a 300-mL linear concentration gradient starting with chromatography buffer containing 0.05 M potassium chloride and ending with buffer containing 0.1 M potassium chloride followed by 100 mL buffer containing 0.1 M potassium chloride. The green fractions containing cytochrome *c* oxidase were pooled and concentrated to >250 μM in cytochrome *c* oxidase with the use of a Centriprep-30 device (Amicon). The concentrated enzyme was rapidly frozen in 100-μL aliquots in cryovials (Nunc) and stored at -80°C. The enzyme prepared in this way exhibited a maximal turnover rate for oxidation of horse heart ferrocytochrome *c* of 570 ± 30 s^{-1} at 25°C and a K_m of 180 ± 20 μM. Analysis by sodium dodecylsulfate polyacrylamide gel electrophoresis showed three components of approximate molecular mass of 52, 30, and 23 kDa.

Preparation of resting and mixed-valence states of cytochrome c *oxidase*

Beef heart or *P. denitrificans* cytochrome *c* oxidase in the resting state was prepared by diluting thawed aliquots of the purified, detergent-solubilized enzyme so that the resulting solution contained 0.167 M sodium sulfate or 0.5 M potassium chloride buffered with 0.05 M HEPES to pH 7.4 and

containing either 0.1% (w/w) or 0.5% (w/w) lauryl-β-D-maltoside. The mixed-valence $a^{2+}a_3^{3+}$·$HCOO^-$ state of the enzyme was prepared by adding ammonium or sodium formate (Sigma) to a final concentration of 0.01 M, followed by addition of the sodium salt of L-ascorbic acid (Sigma). The salts were added either as solids or in small aliquots of freshly prepared, concentrated stock solutions. The $a^{2+}a_3^{3+}$·$HCOO^-$ state prepared in this manner was stable for several days when kept at 0°C. Addition of TMPD led to more rapid formation of the $a^{2+}a_3^{3+}$·$HCOO^-$ state but also led to subsequent formation of the fully reduced $a^{2+}a_3^{2+}$ form followed by the appearance of the $a^{3+}a_3^{3+}$·$HCOO^-$ state of the enzyme. The fully oxidized $a^{3+}a_3^{3+}$·CN^- form of the enzyme was prepared by adding solid potassium cyanide (Aldrich Chemical Co., Milwaukee, WI) to the resting enzyme to a final concentration of 0.01 M. Samples were typically incubated on ice for 20 h to ensure complete binding. The mixed-valence $a^{2+}a_3^{3+}$·CN^- state of the enzyme was prepared by adding to $a^{3+}a_3^{3+}$·CN^- in solution either solid sodium dithionite (Sigma) under nitrogen to 0.01 M final concentration or a combination of L-ascorbic acid to 0.01 M final concentration with 10^{-5} M TMPD.

Preparation of the fully reduced state of cytochrome c oxidase

The fully reduced $a^{2+}a_3^{2+}$ state of the enzyme from either species was prepared by equilibrating a solution of the resting enzyme with an oxygen-free atmosphere of either nitrogen or argon followed by addition of either a small excess of solid sodium dithionite or L-ascorbate and 10^{-5} M TMPD. Reduction was complete in 20 min. The $a^{2+}a_3^{3+}$·CO state of the enzyme was prepared by introducing gaseous carbon monoxide (99.99%, Matheson, Montgomeryville, PA) into the solution. Incubation was allowed to continue for 20 min to ensure complete saturation of binding sites by carbon monoxide.

Methods

Absorption spectroscopy at room temperature

A Cary-14 spectrophotometer modified for microprocessor controlled data collection by On-line Instrument Systems, Inc. (Jefferson, GA) was used to measure electronic absorption spectra at room temperature. A stopcock valve fused to a cuvette with a 1-cm path length allowed for efficient exchange of gases, and the cuvette was maintained at 19.0 ± 0.1°C with the use of a circulating, constant temperature water bath. Absorption spectra were recorded as the average of 10 scans. For each of these 10 scans, absorption data points at intervals of 0.2, 0.5, or 1.0 nm were measured as the average of five readings. The reference spectrum of an appropriately prepared blank was digitally subtracted. Second derivative spectra were calculated by the algorithm of Savitzky and Golay (Savitzky and Golay, 1964) as described in this article, with use of a C language computer program, which allowed the spectral width of the computational filter to be adjusted to maximize resolution, accuracy, and signal-to-noise ratio (Horvath, 1994).

Absorption spectroscopy at 77 K

An Aminco split beam DW-2 spectrophotometer with digital upgrade (On-line Instrument Systems, Inc.) in the laboratory of Professor Robert Gennis at the Department of Chemistry, University of Illinois, Urbana, IL, was used for measuring electronic absorption spectra at 77 K. The sample, prepared in an anaerobic vial, was transferred to one of two chambers between two Plexiglas plates separated by a 0.1-cm copper plate. The second chamber was filled with a blank solution. The sample and blank were frozen by placing the end of the copper plate in liquid nitrogen contained in an evacuated glass dewar. The highly scattering, cracked, frozen solution that formed on freezing had an effective path length approximately fivefold greater than that of a liquid sample. Absorption spectra were recorded as described for spectra of samples at room temperature except that the digital subtraction of a reference blank was not required. Occasionally, a new crack would form in the blank or the sample, causing a shift in the offset of the spectrum during data collection. In such cases, data collection was terminated and a new spectrum was recorded.

Absorption spectroscopy at variable temperatures

A Cary-14 spectrophotometer in the laboratory of Professor Hans Frauenfelder in the Department of Physics at the University of Illinois at Urbana was used for measuring the electronic absorption spectrum of cytochrome *c* oxidase at temperatures between 298 and 10 K. Samples prepared for variable temperature spectroscopy contained 75:25 (w/w) glycerol:water so that the samples formed a translucent glass with no cracks at temperatures below 160 K. Samples prepared in anaerobic vials were transferred to completely fill a plastic cuvette previously sealed with a plug of silicone rubber and flushed with nitrogen gas. The cuvette was mounted to the sample holder and enclosed in a sealed chamber, and the entire assembly was lowered into position in the light path of the spectrophotometer. A helium cryostat (Lake Shore Cryotronics, Columbus, OH) was used to regulate the temperature between 298 and 10 K. The temperature was measured with the use of a calibrated diode thermocouple. For temperatures above 180 K, the chamber enclosing the sample was flushed with dry nitrogen, and for temperatures below 180 K it was evacuated. Electronic absorption spectra were recorded as described for spectra of samples at room temperature, except that a neutral density filter was placed in the reference beam so that the offset of the absorption spectrum was close to zero.

QUANTITATIVE ANALYSIS OF DIRECT AND SECOND DERIVATIVE ELECTRONIC ABSORPTION SPECTRA

Simplified least-squares method for the calculation of second derivative absorption spectra

Historically, second derivative electronic absorption spectra have been obtained either with electronic differentiators (Martin, 1957; Green and O'Haver, 1974) or with wavelength modulators (Bonfiglioli and Brovetto, 1964; Williams and Hager, 1970). With the increased availability of microprocessor-controlled spectrophotometers, it is now possible to record an absorption spectrum in a computer-readable format, and to calculate the second derivative with use of numerical methods such as the simplified least-squares method of Savitzky and Golay (1964) or by differentiation in the Fourier domain (Kauppinen et al., 1981b; Cameron and Moffat, 1984, 1987; Mantsch et al., 1988). Of these two numerical methods, the simplified least-squares method is computationally more efficient. All of the second derivative absorption spectra reported here were, therefore, obtained by the simplified least-squares method of Savitzky and Golay (1964).

In applying the simplified least-squares procedure, the second derivative spectrum is calculated as the convolution of the absorption spectrum with the Savitzky–Golay filter, described by a set of N values $\{w_i\}$, according to

$$A''_j = (\Delta p \Delta x)^{-2} \sum_{i=-(N-1)/2}^{(N-1)/2} w_i A_{(j+i\Delta p)}. \quad (1)$$

In this expression, A''_j is the second derivative at the jth position in the spectrum, Δx is the separation between data points measured in units of cm^{-1}, Δp is the integral number of data points spanned by the interval of differentiation, and $A_{(j+i\Delta p)}$ is the absorption value measured at position $(j + i\Delta p)$ in the spectrum. The set of values $\{w_i\}$ that define a Savitzky–Golay filter are derived with the use of linear algebra (Savitzky and Golay, 1964; Steiner et al., 1972), and a suitable example of the approach used to derive $\{w_i\}$ can be examined in the Appendix. Numerical details of the method of calculating the second derivative spectrum are illustrated in Fig. 1.

The convolution described by Eq. 1 uses absorption values in a neighborhood that is centered on the jth position of the spectrum and that extends over a spectral width ϕ defined by

$$\phi = (N - 1)\Delta p \Delta x. \tag{2}$$

Recording the absorption spectrum with different Δx, applying a filter using different values of Δp, or applying a filter described by a different number of values N will produce differences in the signal-to-noise and accuracy of the second derivative spectra.

Signal-to-noise and accuracy

Selection of appropriate experimental parameters has been described for wavelength modulation spectroscopy (Cahill, 1979; Cahill and Padera, 1980) and for differentiation in the Fourier domain (Kauppinen et al., 1981a,b; Cameron and Moffat, 1984, 1987; Mantsch et al., 1988). Here, parameters particular to the calculation of second derivative spectra by the simplified least-squares method of Savitzky and Golay (1964) are discussed. Achieving adequate signal-to-noise depends critically on the spectral width ϕ and the number of values N used to describe the Savitzky–Golay filter. Also, the accuracy of the second derivative calculation depends on matching the spectral width of the filter with the bandwidth of the spectral features in the absorption spectrum. The results presented here lead to a set of rules that ensure that an appropriate approximation is obtained with use of the simplified least-squares method.

Noise in the second derivative spectrum increases as the inverse square of the spectral width of the filter ϕ, and, for filters with equivalent values of ϕ, the noise will be least for that filter described by the largest number of values N. These observations were made by analyzing absorption spectra that were generated using a computer program (Horvath, 1994). The computer program was designed so that the collection of absorption values that make up the absorption spectrum should approximate a normal distribution. Thus, the computer-generated absorption spectra consisted of random noise characterized by a normal distribution of values. The second derivative spectra were calculated according to Eq. 1 using different Savitzky–Golay filters with values of N ranging from 5 to 25. The spectral width ϕ of the filter was adjusted by selecting different values of Δp. The noise in the absorption spectrum σ and in the second derivative spectrum was measured as the sample standard deviations of the absorption and second derivative values. Figure 2 shows the inverse square relationship of σ'' and ϕ found for several different filters that is expressed by

$$\sigma'' = \sigma\left(\frac{\rho_N}{\phi^2}\right). \tag{3}$$

For each filter, the proportionality coefficient can be calculated exactly according to

$$\rho_N = \frac{\sqrt{\sum w_i^2}}{(N-1)^2}. \tag{4}$$

Eq. 4 was derived on the basis of error analysis of Eq. 1 (Horvath, 1994). Values of calculated ρ_N using Eq. 4 are given in Table 1.

These results explain the seemingly incongruous observation that the signal-to-noise ratio of the second derivative spectrum decreases as data are collected with closer spacings (i.e., smaller Δx). Most commercially available programs that calculate the second derivative spectrum assume that $\Delta p = 1$. Therefore, by decreasing Δx, ϕ will decrease, and noise in the second derivative will increase according to Eq. 3. To circumvent this problem, Δp should be increased for a corresponding decrease in Δx. For instance, if the spectrum is collected at 0.2-nm intervals, then Δp must be increased fivefold for the second derivative to have the same signal-to-noise ratio as a spectrum collected with 1.0-nm intervals, as required by Eq. 2. For this reason, all of the second derivative spectra reported in this work were calculated with the use of a program (Horvath, 1994) that implements Eq. 1 and allows the user to specify Δp. The C language code for this program is given in Appendix II of Horvath (1994).

The high level of noise in second derivative spectra calculated with narrow Savitzky–Golay filters (small values of ϕ) is closely parallel to the high level of noise in second derivative spectra obtained with the use of wavelength modulation spectroscopy if the range of the wavelength modulator is narrow (Cahill, 1979; Cahill and Padera, 1980). An error analysis of second- and higher-order derivative spectra treats the operation of differentiation as a series of subtraction and division operations followed by a simple average-smoothing operation (O'Haver and Begley, 1981). In contrast, the simplified least-squares method (Savitzky and Golay, 1964) applied here incorporates smoothing directly into the operation of calculating the second derivative. Therefore, the description of errors is different for the simplified least-squares method. However, the analogy to simple mathematical operations of subtraction, division, and averaging is useful in understanding the effect of filter width ϕ on the noise in second derivative spectra. Choosing a small interval of differentiation ($\Delta p \Delta x$, see Fig. 1) magnifies the error incurred during the subtrac-

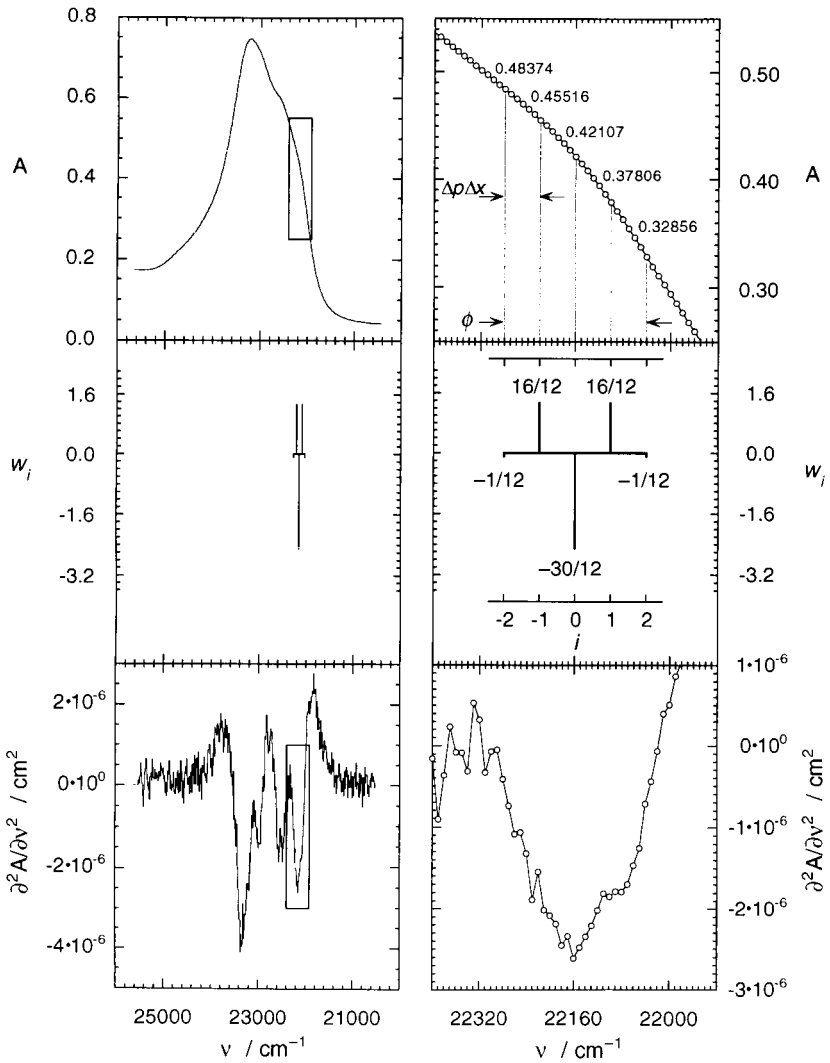

FIGURE 1 Simplified least-squares procedure for the calculation of a second derivative spectrum. The absorption spectrum of carbon-monoxide-bound cytochrome *c* oxidase is shown in the top set of panels. The corresponding second derivative spectrum is shown in the bottom set of panels. In each case, the right-hand panel is an expanded view of the area boxed in the left-hand panel. The second derivative spectrum was calculated as the convolution of the Savitzky–Golay filter, shown in the middle panels, with the absorption spectrum. The calculation of the second derivative at 22,160 cm^{-1} is carried out explicitly in the following equation. Each of the indicated absorption values (*top, right-hand panel*) is multiplied by the value of the filter at the corresponding position (*middle, right-hand panel*), and the sum of these terms is scaled (see below) to give the value of the second derivative at 22,160 cm^{-1} (A''_{22160}) with appropriate units.

$$A''_{22160} = \left(60\ \mathrm{cm}^{-1}\right)^{-2} \times \begin{bmatrix} -1/12 & (0.48374 + 0.32856) \\ +16/12 & (0.45516 + 0.37806) \\ -30/12 & (0.42107) \end{bmatrix}$$

$$= -2.6130 \times 10^{-6}\ \mathrm{cm}^2.$$

The filter chosen for this example is defined by a set of $N = 5$ values. The spacing between data points (Δx) is 10 cm^{-1}. The number of data points per interval of differentiation (Δp) is chosen to be 6. Therefore, the separation between points ($\Delta p \Delta x$) used in the calculation of the second derivative is 60 cm^{-1} as indicated in the enlarged view of the absorption spectrum. In transferring from the domain of the filter (i) to the domain of the absorption data (cm^{-1}), a scaling factor $(\Delta p \Delta x)^{-2} = (60\ cm^{-1})^{-2}$ is introduced. The spectral width of the filter ϕ, as applied here, is $(N - 1)\Delta p \Delta x = 240\ cm^{-1}$, which is less than the bandwidth of the feature $\Gamma \cong 540\ cm^{-1}$ (see text).

tion operation because the denominator in the division operation is small. Thus, as Δx decreases without a compensatory increase in Δp, signal-to-noise will suffer. By choosing a large value for $\Delta p \Delta x$, the error of the subtraction operation will be minimized. Choosing a Savitzky–Golay filter with N large effectively increases the window over which the result is smoothed. Thus, noise is diminished with increasing N. This property is reflected by the decrease in the proportionality constant of Eq. 3 as N increases (cf., Table 1).

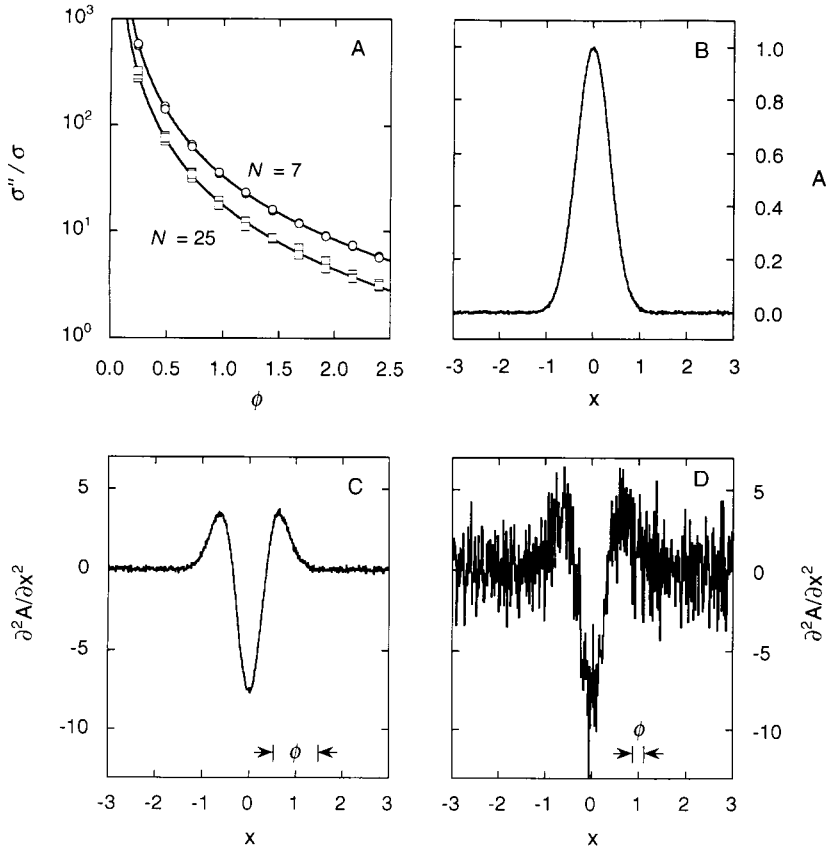

FIGURE 2 Relationship of noise in the second derivative spectrum to ϕ, the spectral width of the Savitzky–Golay filter. (*A*) The increase in noise incurred by applying the second derivative operation, quantified as the ratio σ''/σ, is plotted as a function of ϕ for Savitzky–Golay filters defined by $N = 7$ (*circles*) or $N = 25$ (*squares*). For each value of ϕ, three independent spectra were analyzed to give three independent determinations of σ''/σ. To calculate σ''/σ, absorption spectra were simulated as random, normally distributed values and the sample standard deviation in the second derivative spectrum was divided by the sample standard deviation of the absorption spectrum. The solid curves are theoretical curves generated by Eqs. 3 and 4 that are derived from error analysis considerations that apply to Eq. 1. To illustrate the effect of the choice of ϕ on the noise apparent in the second derivative spectrum, the second derivative of a Gaussian distribution with bandwidth $\Gamma = 1$, shown in panel *B*, was calculated with the use of a Savitzky–Golay filter of $N = 7$ values with $\phi = 0.96$ (panel *C*) or $\phi = 0.24$ (panel *D*). Decreasing ϕ dramatically increases the noise level in the second derivative spectrum. The randomly distributed noise present in the absorption spectrum (*B*) has a sample standard deviation of 0.0028. From Eq. 3 and values of ρ_N reported in Table 1, the sample standard deviation of the noise present in the second derivative spectra can be calculated as 0.10 in panel *C* and 1.6 in panel *D*.

From the above consideration of signal-to-noise, it is desirable to use a filter characterized by large spectral width ϕ and a large number of points N. Consideration of accuracy, discussed below, shows that ϕ must be matched to the bandwidth Γ of the narrowest feature of interest in the absorption spectrum. This result is found to be independent of the number of values N used to describe the filter (Horvath, 1994). Accuracy was evaluated by comparing the values of the second derivative calculated using Eq. 1 with known values. To obtain known values of the second derivative, an absorption spectrum was modeled as a Gaussian distribution according to

$$f_G(x; A_0, x_0, \Gamma) = A_0 \exp\left(-\frac{4(x - x_0)^2}{\Gamma^2}\right), \qquad (5)$$

and the second derivative was calculated according to

$$f''_G(x) = -\frac{8}{\Gamma^2}\left[1 - \frac{8(x - x_0)^2}{\Gamma^2}\right] f_G(x; A_0, x_0, \Gamma), \qquad (6)$$

where $f_G(x; A_0, x_0, \Gamma)$ is the Gaussian distribution characterized by maximum amplitude A_0, position of maximum amplitude x_0, and linewidth Γ measured as the distance

TABLE 1 Values of ρ_N for Savitzky–Golay filters defined by *N* points

N	ρ_N
5	50.1
7	33.3
9	28.4
11	25.6
13	23.6
15	22.1
17	20.9
19	19.9
21	19.0
23	18.3
25	17.6

between the two points where the function is equal to A_0/e. The second derivative of the Gaussian distribution $f''_G(x)$ is, thus, described by the same parameters as is the Gaussian distribution itself.

Accuracy was then evaluated according to

$$\text{accuracy} = 1 - \sqrt{\frac{\sum (A''_i - A''_{c_i})^2}{\sum A''^2_i}}, \qquad (7)$$

where A''_i is the known value of the second derivative at the ith position in the spectrum and A''_{c_i} is the value of the second derivative at the ith position approximated with use of the simplified least-squares method.

Accuracy drops dramatically if the spectral width of the filter ϕ is larger than the bandwidth of the Gaussian distribution Γ, as seen in Fig. 3. This result closely resembles the observation that, when wavelength modulation is applied to obtain the second derivative spectrum, line shape distortions are more pronounced if the spectral band-pass is larger than the widths of the features in the spectrum (Cahill and Padera, 1980). The simplified least-squares method effectively models the absorption values within the spectral width of the filter as a quartic polynomial (Savitzky and Golay, 1964; see also Appendix). In this manner, the second derivative calculation is smoothed over the spectral width of the filter. If smoothing is extended beyond the neighborhood of a feature by applying too broad of a filter, then the second derivative calculation will be inaccurate.

To achieve the maximum signal-to-noise ratio, the Savitzky–Golay filter with the broadest spectral width ϕ should be applied. However, to maintain accuracy, a narrow filter is required. Accuracy suffers the most when ϕ is greater than the bandwidth Γ of the feature, as illustrated in

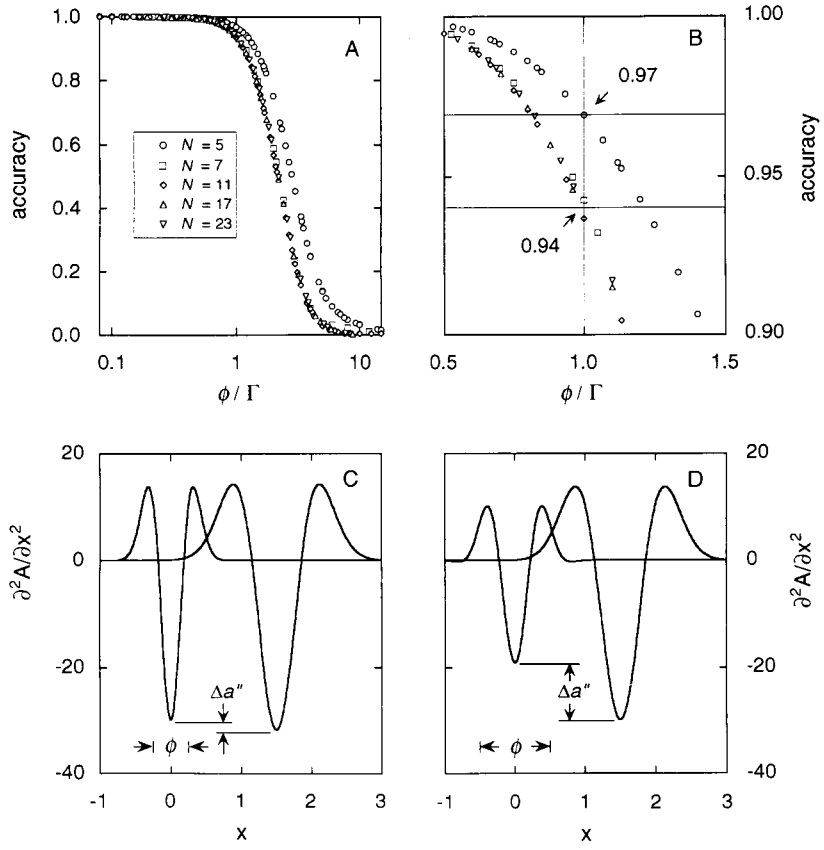

FIGURE 3 Relationship of accuracy of the numerical calculation of the second derivative spectrum to ϕ, the spectral width of the Savitzky–Golay filter. (*A* and *B*) Accuracy of the second derivative calculation is plotted as a function of ϕ for Savitzky–Golay filters defined by $N = 5$ (*circles*), $N = 7$ (*squares*), $N = 11$ (*diamonds*), $N = 17$ (*triangles*), and $N = 23$ (*inverted triangles*). Note that accuracy, calculated according to Eq. 7, decreases as ϕ increases. An accuracy of 1.0 means that the calculated and known values of the second derivative spectrum agree exactly. An accuracy of 0.0 means that the second derivative calculation was insensitive to any changes in curvature present in the absorption spectrum. (*B*) An expanded view of a portion of the data presented in panel *A*. For $\phi/\Gamma > 1.0$, accuracy is low and is dependent on the number of points defining the filter. If $\phi/\Gamma = 1.0$, accuracy obtained with a filter defined by $N = 5$ points is 0.97, and the accuracy obtained with filters defined by $N \geq 7$ points is 0.94. If, in contrast, $\phi/\Gamma < 1.0$ then accuracy is always greater than 0.95. To illustrate the effect of ϕ on quantitative analysis, the second derivative of two Gaussian distributions of unequal bandwidths was evaluated using different values of ϕ. (*C*) The spectral width ϕ of the Savitzky–Golay filter was chosen to match the bandwidth of the narrowest distribution. (*D*) ϕ was chosen to match the bandwidth of the broadest distribution. If the second derivative calculation were exact, the two features present in the second derivative spectrum would have equal trough values. The degree to which the trough values differ ($\Delta a''$) reflects the degree of inaccuracy of the second derivative calculation. Inaccuracy is minimized by choosing ϕ to be less than or equal to the bandwidth of the narrowest feature of the absorption spectrum. (*C*) $\Delta a''$ is 6% of the true trough value. (*D*) $\Delta a''$ is 36% of the true trough value.

Fig. 3. Thus, an appropriate choice of parameters to calculate the second derivative spectrum can be made by choosing a filter with the largest spectral width ϕ that is still smaller than the bandwidth Γ of the narrowest feature of interest in the spectrum.

Table 1 and Fig. 3 show that, in addition to the choice of ϕ, the compromise between signal-to-noise and accuracy can be influenced by the choice of N. As N increases, the noise in the second derivative spectrum decreases (cf., Table 1). Therefore, noise in the second derivative can be suppressed by measuring the absorption spectrum with small values of Δx so that filters with large N can be applied to calculate the second derivative without exceeding the constraint of keeping ϕ smaller than Γ. For equivalent values of ϕ, accuracy is slightly greater when the second derivative spectrum is calculated with the use of a Savitzky–Golay filter defined by $N = 5$ (cf., Fig. 3). Slightly lower values of accuracy were obtained for the other filters defined by $N \geq 7$.

Resolution

In addition to influencing signal-to-noise and accuracy, the spectral width ϕ of the Savitzky–Golay filter also determines the resolution enhancement realized in the second derivative spectrum. This aspect was particularly important in the analysis of the absorption spectra of cytochrome *c* oxidase. Resolution of features present in the second derivative spectrum improves as ϕ decreases. The effect of band-pass on resolution of components in second derivative spectra obtained with the use of wavelength modulation spectroscopy shows a similar behavior (Cahill and Padera, 1980). When too broad of a filter is applied, as shown in

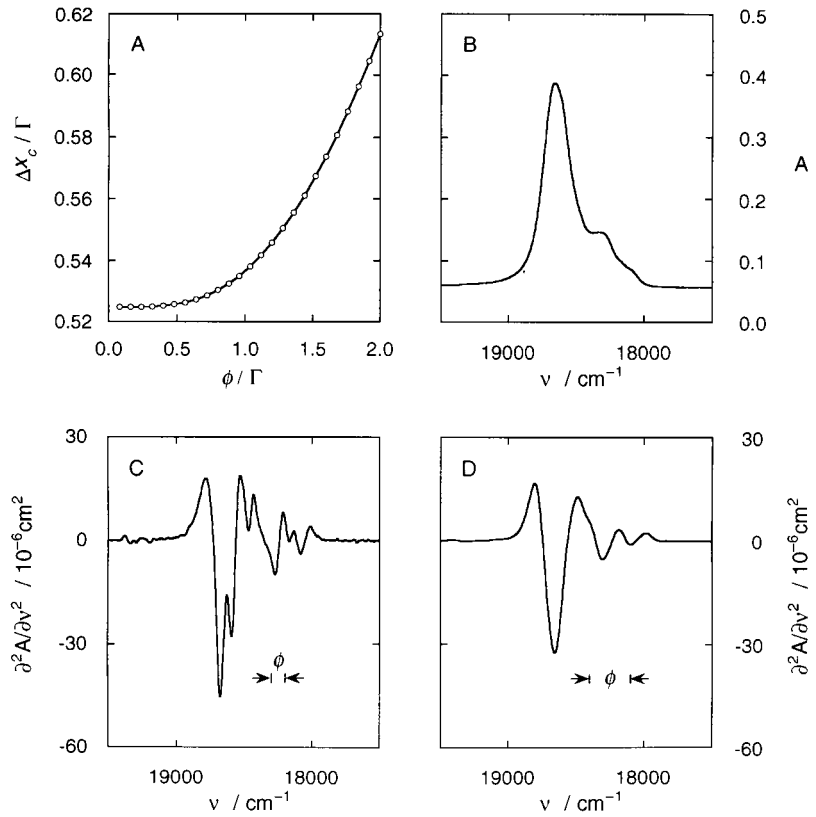

FIGURE 4 Influence of ϕ, the spectral width of the Savitzky–Golay filter, on the number of features resolved in the second derivative spectrum. (*A*) As ϕ increases, the separation Δx_c of two Gaussian distributions of equal width Γ and amplitude needed to be able to detect two relative minima in the second derivative spectrum also increases. If the two Gaussian distributions are separated by less than Δx_c, then only one relative minimum is observed in the second derivative spectrum. For comparison, the separation required to observe two relative maxima in the absorption spectrum is $\Delta x_c = 0.707\ \Gamma$. The theoretical limit to Δx_c, attainable with small values of ϕ, is $0.525\ \Gamma$. In the case that ϕ is equal to Γ, Δx_c is $0.536\ \Gamma$, meaning that 6% of the theoretical advantage gained by the second derivative operation is lost as a consequence of the inaccuracy of the numerical calculation. In the case that ϕ is equal to $2\ \Gamma$, Δx_c is $0.613\ \Gamma$, meaning that 49% of the theoretical advantage gained by the second derivative operation is lost. The width and amplitude defining the two Gaussian distributions used in this example are equal. Similar results are obtained using two distributions with unequal widths and amplitudes. The number of features that are resolved in the second derivative spectrum depends on the choice of ϕ. (*B*) The absorption spectrum of holmium oxide from 19,500 to 17,500 cm^{-1}. Three components are detectable in the absorption spectrum as relative maxima or points of inflection. In the second derivative spectrum, six features are detectable as relative minima if ϕ is chosen to be 100 cm^{-1} (panel *C*), but only three features are detectable if ϕ is chosen to be 300 cm^{-1} (panel *D*). Each second derivative spectrum was calculated with use of a Savitzky–Golay filter defined by $N = 11$ values and ϕ was adjusted by varying Δp.

Fig. 4, features in the second derivative spectrum are lost. Because the second derivative spectrum is often used to determine the number and positions of absorption components (Pleshko et al., 1991; Sherman et al., 1991; Kaschny and Goñi, 1992; Lynch et al., 1992; Copeland, 1993; Torres and Padrós, 1993), it is important to choose an appropriate value for ϕ to avoid under-estimation of the number of such components.

To evaluate the minimum value of ϕ required to maintain high quality of resolution attainable in second derivative spectra, absorption spectra were simulated as the sum of two Gaussian distributions of equal bandwidth. For different values of ϕ, the distance separating the two distributions was varied to determine the critical separation Δx_c at which two troughs, and not one, could be detected in the second derivative spectrum. These results are also shown in Fig. 4. If ϕ is chosen to be small relative to the bandwidth Γ of the Gaussian distribution, then Δx_c approaches a theoretical limit of 0.525 Γ. For comparison, the critical separation required to observe two maxima, and not one, in the absorption spectrum is 0.707 Γ. If the criterion, established above, that ϕ should be matched with the bandwidth of the narrowest feature in the spectrum is applied, then Δx_c is equal to 0.536 Γ. Such a modest increase in Δx_c does not adversely affect resolution; and, therefore, the criterion for parameter selection derived on the basis of considering signal-to-noise and accuracy is also appropriate on the basis of considering resolution.

Rules for parameter selection in the calculation of second derivative absorption spectra

The results reported above can be summarized as a set of three rules for the selection of parameter values included in the simplified least-squares method for calculation of second derivative absorption spectra: 1) Signal-to-noise improves as the number of points in the filter increases and as the width of the filter increases; therefore, filters characterized by large N and ϕ should be selected to improve signal-to-noise. 2) Accuracy increases and resolution of features in the second derivative spectrum improves as the filter width decreases; therefore, filters characterized by small ϕ should be selected to improve accuracy and resolution. 3) To arrive at an acceptable compromise between the competing goals of achieving adequate signal-to-noise versus high accuracy and resolution, ϕ should be chosen so that $\phi \leq \Gamma_{min}$ where Γ_{min} is the linewidth of the narrowest feature of interest in the second derivative spectrum.

In applying Rule 3 above, it is necessary to estimate linewidths of features apparent in the second derivative spectrum. Quantitative analysis of absorption and second derivative absorption spectra described below can be applied to obtain linewidths of components. A quick estimate of the linewidth of a well-resolved feature in the second derivative absorption spectrum can also be obtained by measuring the distance between the position of a side peak and the trough (Δx_{pt}) and using

$$\Gamma = \sqrt{\frac{8}{3}}\,\Delta x_{pt} \tag{8}$$

to estimate Γ. Eq. 8 was derived by defining the points where the third derivative of the Gaussian distribution function acquires a value of zero. All of the second derivative absorption spectra described or reported in this work were obtained with application of the three rules described above.

Parameterization of absorption and second derivative spectra

To parameterize spectra, a model of the direct and second derivative absorption spectra was constructed as the sum of components, each described by a Gaussian distribution. The values of the parameters specifying the maximum amplitude, position, and linewidth of each component were iteratively adjusted by the algorithm of Marquardt (1963) until the sum of squared residuals of both the direct absorption and the second derivative data were minimized. The number of components used to model the direct absorption and second derivative spectra was adjusted until the direct absorption and second derivative residuals no longer showed distinct features above the level of noise. At this point, the model was further tested by removing components until the fit of the model to the data suffered noticeably. The minimum number of components necessary to simulate the direct and second derivative spectra was determined in this manner. The uncertainty in the values of parameters obtained from quantitative analysis was determined as described previously (Horvath, 1994) and is a measure of the variability in parameter values expected from random fluctuations in absorption values and does not include variability dependent on the starting point of minimization or on the number of components incorporated in the model. General conclusions reached on the basis of quantitative analysis of direct and second derivative spectra were confirmed by parallel analyses, which incorporated a different number of components or which modeled the data using the same number of components but in quantitatively different combinations.

RESULTS

Low-temperature spectroscopy of formate-bound cytochrome *c* oxidase

Figure 5 compares the direct and second derivative absorption spectra of the $a^{2+}a_3^{3+}$·$HCOO^-$ form of beef heart cytochrome *c* oxidase at three temperatures. By adding ascorbate to formate-bound cytochrome *c* oxidase, a mixed-valence state of the enzyme can be stabilized in which cytochrome a_3 contains a high-spin Fe^{3+} ion bound to formate while cytochrome *a* contains a low-spin Fe^{2+} ion (Nicholls, 1976). In this state, the Soret absorption spectrum

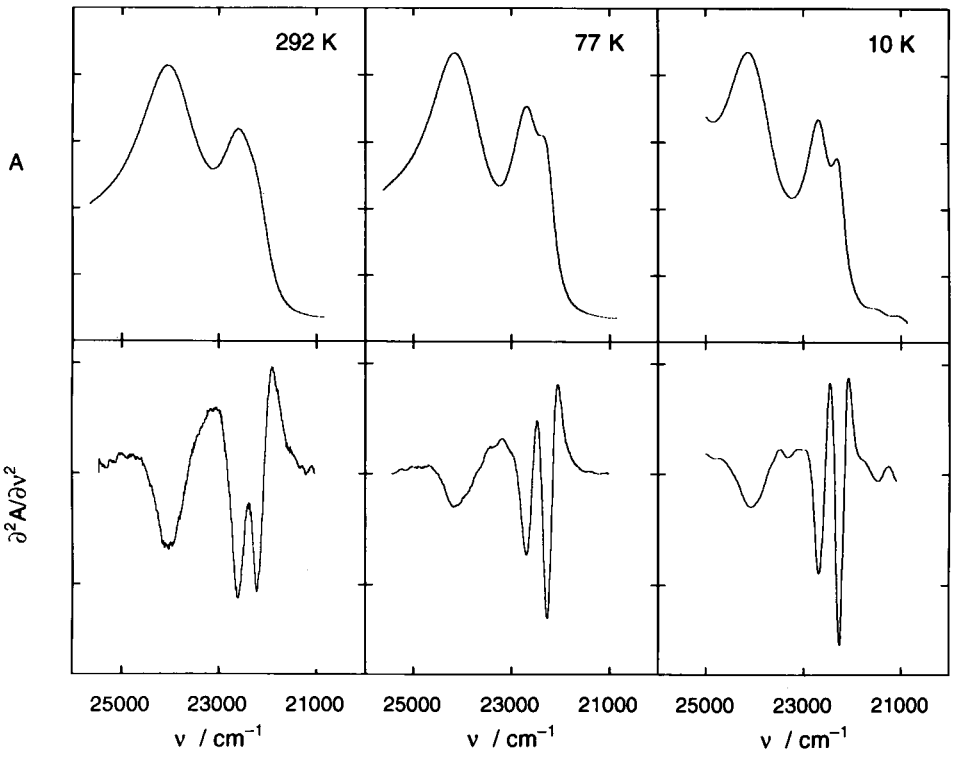

FIGURE 5 Direct and second derivative absorption spectra of the mixed-valence $a^{2+}a_3^{3+}$·$HCOO^-$ form of beef heart cytochrome *c* oxidase at 292, 77, and 10 K. The sample at 292 K is a fluid aqueous suspension, the sample at 77 K is a frozen solution, and the sample at 10 K is prepared as a glass consisting of 75:25 (w/w) glycerol:water. In the direct absorption spectrum, the component at 24,100 cm^{-1} is due to cytochrome a_3, which contains a high-spin Fe^{3+} ion, and the spectral features centered at 22,600 cm^{-1} are due to cytochrome *a* with a low-spin Fe^{2+} ion (Nicholls, 1976). As the temperature is lowered, the two-component nature of the direct absorption spectrum of cytochrome *a* becomes increasingly apparent. The second derivative spectrum reveals the changes in curvature at all temperatures to identify both features with significant signal-to-noise. The absorption measurements and corresponding second derivative are plotted on a relative scale because different samples were used at each temperature.

of cytochrome a_3 is maximally displaced from the absorption spectrum of cytochrome *a*, so that, at room temperature, two maxima are observed in the direct absorption spectrum in the Soret region. As the temperature is lowered, the direct absorption spectrum of cytochrome *a*, centered at 22,600 cm^{-1} (442 nm), is progressively split into two components with maxima at 22,700 cm^{-1} (441 nm) and 22,300 cm^{-1} (448 nm) so that, at 10 K, the two features are distinctly identified as separate but overlapping absorption bands. Although the second derivative spectrum similarly identifies two components centered near 22,600 cm^{-1} at 10 K, it is seen that the second derivative spectrum remains sensitive to the changes in curvature at higher temperatures, in particular at 292 K, where the direct absorption spectrum yields only a slight hint of a second component associated with the main feature at lower energy attributed to cytochrome *a*. These two features identified through second derivative spectroscopy were first assigned to ferrocytochrome *a* (Sherman et al., 1991).

Low-temperature spectroscopy of unliganded cytochrome *c* oxidase

To test whether ligand binding at cytochrome a_3 is a requirement to elicit the doublet features near 440 and 450 nm ascribed to cytochrome *a*, a study of the unliganded enzyme at cryogenic temperatures was carried out. As shown in Fig. 6, the doublet features at 440 and 450 nm are not resolved in the second derivative spectrum of beef heart cytochrome *c* oxidase at room temperature, but the doublet features are observed in the second derivative absorption spectrum of the unliganded enzyme at cryogenic temperatures. Similar results were obtained for *P. denitrificans* cytochrome *c* oxidase.

As shown in the preceding section, the presence and trough depth of a second derivative absorption feature depend on both the amplitude and linewidth of the absorption band that gives rise to the feature (cf., Eq. 6). That the 450 nm feature is observed in second derivative absorption spectra of the unliganded enzyme at 77 K but not in spectra of the unliganded enzyme at room temperature could be the consequence of either the temperature dependence of the amplitude of the absorption component at 450 nm or the result of an improvement in resolution of absorption components due to narrower linewidths at lower temperatures.

To test which mechanism best accounts for the temperature dependence of second derivative spectra of the unliganded enzyme, direct absorption and second derivative spectra of the unliganded enzyme at several temperatures ranging from 20 to 298 K were analyzed. Figure 6 shows the results of analyzing the direct absorption and second derivative spectra of unliganded beef heart cytochrome *c* oxidase at 298, 200, and 20 K. For application of mathematical parameterization of the direct and second derivative absorption spectra, each direct absorption spectrum was modeled as the superposition of seven Gaussian components. The integrated absorption intensities of each of components 1–4 were held constant with respect to temperature. Constraining the analysis in this manner tests whether the data are consistent with the assumption that the integrated absorption intensity remains constant with temperature. In a parallel analysis, no such restriction was placed on the

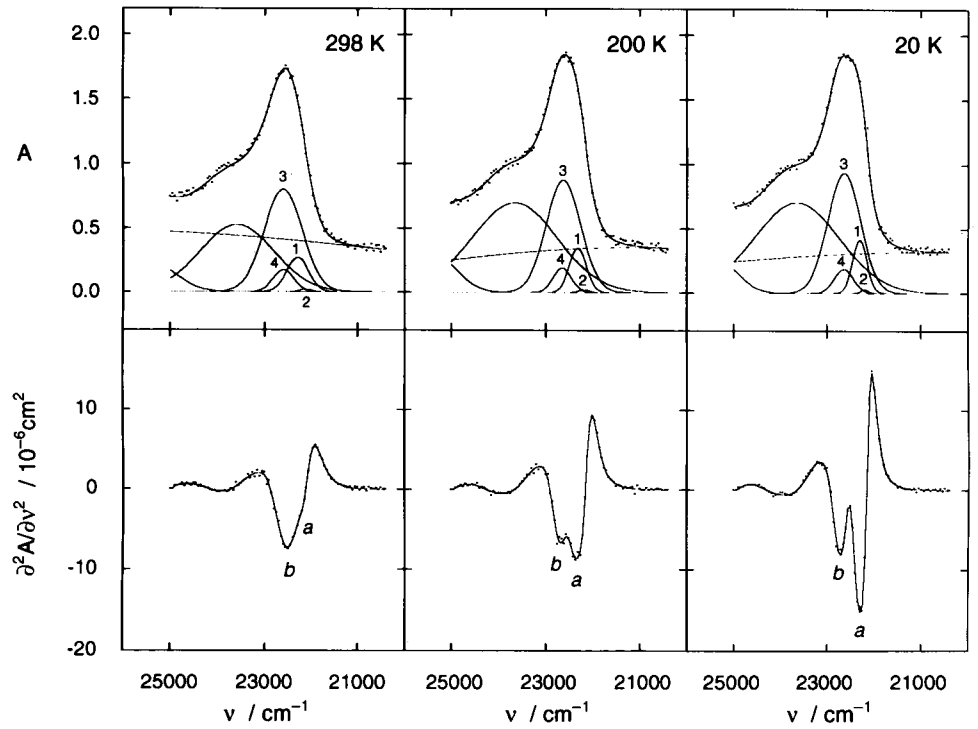

FIGURE 6 Analysis of the direct and second derivative absorption spectra of the $a^{2+}a_3^{2+}$ state of beef heart cytochrome *c* oxidase. A sample of beef heart cytochrome *c* oxidase was prepared as the fully reduced, unliganded $a^{2+}a_3^{2+}$ state in a solution of 75:25 (w/w) glycerol:water buffered to pH 7.4 with 0.05 M HEPES. The spectra recorded at 298, 260, 200, 140, 80, and 20 K were together analyzed as a set of data. Results from analysis of the sample at three of the six temperatures (298, 200, and 20 K) are displayed here. Each direct absorption spectrum was modeled as the superposition of seven absorption components. Of these seven components, components 1–4 modeled features *a* and *b* resolved at low temperatures. The integrated absorption intensity of each of these four components was constrained to be constant with temperature. Under this constraint, changes in position and changes in linewidth with corresponding changes in amplitude account for the temperature-dependent changes in the direct and second derivative absorption spectrum. To present experimental and model spectra, the experimental data points were scattered by approximately 2% of the overall absorption range. This variance was introduced exclusively for purposes of comparing the observed absorption spectrum to the calculated spectrum obtained by mathematical modeling. It does not influence the course of the analysis. Model spectra are displayed as solid curves with underlying components. A similar method of illustrating experimental and model spectra is applied in subsequent figures.

integrated absorption intensities of the absorption components. As judged by the quality of the fit to the data quantified by the sum of squared residuals, both analyses accounted equally well for observed differences in appearance of the absorption and second derivative absorption spectra. Therefore, the data are consistent with no change in integrated absorption intensity for the 440- and 450-nm components as a function of temperature.

As shown in Fig. 6, all of the changes observed for the features at 440 and 450 nm are accounted for by changes in linewidths of the underlying absorption components. The absorption component at 450 nm (component 1 in Fig. 6) is characterized by the most temperature-sensitive linewidth. The behavior of linewidth with respect to temperature for component 1 is plotted in Fig. 7. Above 150 K, the linewidth of component 1 increases linearly with respect to temperature. The temperature 150 K corresponds to the temperature at which the frozen 75% (w/w) glycerol:water solvent undergoes a glass transition (Yannas, 1968; Rasmussen and MacKenzie, 1971). The change in linewidth with temperature was observed to be reversible with respect to either warming or cooling the sample.

Quantifying the effect of ligand binding on the spectrum of cytochrome *a*

To quantify the effect of ligand binding at cytochrome a_3 on the absorption spectrum of cytochrome *a*, mathematical parameterization of the absorption and second derivative spectrum was applied to the spectra of the unliganded and carbon-monoxide-bound forms of beef heart cytochrome *c* oxidase. Results are presented in Table 2 and Fig. 8. In Fig. 8, absorption components 1–3 are included with identical respective intensity in modeling the spectrum of the carbon-monoxide-bound and unliganded enzyme. This corresponds to analysis 1 of Table 2. These components are presumed to arise from the excited electronic state of cytochrome *a* and to account for the doublet features at 440 and 450 nm in the second derivative spectrum of carbon-monoxide-bound cytochrome *c* oxidase. Specifying that the intensities of components 1–3 are invariant with respect to carbon monoxide binding is consistent with the data only if carbon monoxide binding at cytochrome a_3 does not perturb the absorption properties of cytochrome *a*. In analysis 2 of Table 2, the amplitude of the component at 450 nm (component 1) was

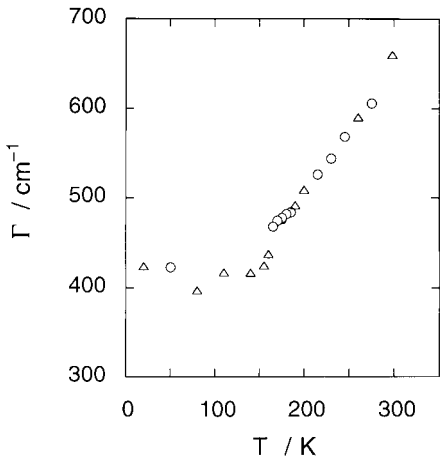

FIGURE 7 Temperature dependence of the linewidth of component 1. The linewidth of component 1 that models feature *a* at 22,300 cm^{-1} (448 nm) in the second derivative spectrum in Fig. 6 is plotted with respect to temperature. Equilibration of the sample at each temperature was for 30 min or longer. Spectra were recorded both after temperature equilibration following a decrease in temperature (*circles*) and following an increase in temperature (*triangles*). To determine linewidth (Γ), spectra were analyzed according to the seven-component model illustrated in Fig. 6. The integrated absorption intensities for components 1–4 were treated as fixed constants equal to the values determined from the analysis shown in Fig. 6. Above 150 K, the linewidth of component 1 increases linearly with temperature. Below this temperature, which corresponds to the glass transition temperature of the 75:25 (w/w) glycerol:water solvent, the linewidth remains constant.

not constrained to be the same for both states of the enzyme. Removing the constraint of equivalent amplitudes tests whether ligand binding at cytochrome a_3 produces measurable differences in the absorption spectrum of cytochrome *a*. As shown in Table 2, when the analysis was carried out without restricting the amplitude of the 450-nm component to be the same for both forms of the enzyme, the intensity of the 450-nm component was, nonetheless, equal for the carbon-monoxide-bound and unliganded form of the enzyme.

In analysis 3 of Table 2, component 1, appearing at 450 nm, was not included in the model of the absorption spectrum of the unliganded enzyme. This analysis tests the hypothesis whether the 450-nm component is entirely dependent on carbon monoxide binding so that the 450-nm component is absent in the unliganded enzyme. As shown in Table 2, the sum of squared residuals measured for analysis 3 is 50% greater than the sum of squared residuals measured for analyses 1 or 2, both of which include the 450-nm component in the absorption spectrum of unliganded cytochrome *c* oxidase. Thus, the 450-nm component is necessary to accurately model the absorption spectrum of the unliganded form of the enzyme. As further evidence, the residuals plotted as a function of wave number showed a feature above the level of noise at 22,100 cm^{-1} if the 450-nm component was omitted as in analysis 3, indicating that the component at 450 nm is present in the spectrum of the unliganded enzyme. Similar results were obtained for the enzyme from *P. denitrificans*, as seen in Table 2.

To test whether a single description of the absorption spectrum of cytochrome *a* could account for the absorption and second derivative spectra of the unliganded ($a^{2+}a_3^{2+}$), carbon-monoxide-bound ($a^{2+}a_3^{2+}\cdot CO$), and cyanide-bound ($a^{2+}a_3^{3+}\cdot CN^-$) states of cytochrome *c* oxidase, direct absorption and second derivative absorption spectra of these three states, were analyzed. Results obtained for the bacterial enzyme from *P. denitrificans* are shown in Fig. 9 and Table 3. Comparable results were also obtained for the beef heart mitochondrial enzyme, as shown in Table 3. In the analysis shown in Fig. 9, absorption components 1–3 are included with identical intensities in all three spectra. A parallel analysis allowed the amplitude of component 1 at 450 nm to vary for the three states of the enzyme. As shown in Table 3, the intensity of the 450-nm component did not depend on the ligand state of cytochrome a_3 (analysis 2 in Table 3) and, as a consequence, very little improvement in the sum of squared residuals was realized by allowing the amplitude of the 450-nm component to vary according to the ligand state of cytochrome a_3.

DISCUSSION

The two-component absorption spectrum of cytochrome *a*

It is well known that the absorption spectra of intact mitochondria at cryogenic temperatures reveal features that are not resolved at room temperature (Wilson and Gilmour, 1967; Wikström et al., 1976). Reduced-minus-oxidized difference spectra of frozen mitochondria inhibited with CN^-, H_2S, CO, or N_3^- are characterized at 77 K by two absorption maxima at approximately 440 and 448 nm (Wilson and Gilmour, 1967). Spectra of mitochondria in steady-state respiration before freezing minus the spectrum of frozen, resting mitochondria show points of inflection at 440 and 450 nm at 77 K (Wikström et al., 1976). These features are at positions similar to those of the doublet features that characterize the second derivative spectrum of ligand-bound forms of cytochrome *c* oxidase (Sherman et al., 1991).

In the present investigation, the spectra of cytochrome *c* oxidase purified from beef heart and from *P. denitrificans* were studied with the goal of further characterizing the doublet features detected in the second derivative absorption spectrum of cytochrome *a* (Copeland, 1991, 1993; Ishibe et al., 1991; Sherman et al., 1991; Lynch et al., 1992; Felsch et al., 1994). In earlier studies of intact mitochondria, collection of difference spectral data was necessary to suppress the absorption contributions of other cytochromes present in mitochondria and the light-scattering contributions from mitochondrial particles (Wilson and Gilmour, 1967; Wikström et al., 1976). In contrast, detergent solubilized preparations of purified cytochrome *c* oxidase, as in the present investigation, allow observation of the direct

TABLE 2 Quantitative analysis of second derivative absorption spectra of $a^{2+}a_3^{2+}$ and $a^{2+}a_3^{2+}$·CO states of beef heart and *P. denitrificans* cytochrome *c* oxidase

Enzyme	Analysis*	$\chi_u^{2\#}$	χ_{CO}^2	$A_{o_1}^u$	$A_{o_1}^{CO}$
Beef heart	1	0.549	1.014	0.061 (6)	0.061 (6)
	2	0.549	1.014	0.061 (7)	0.061 (6)
	3	0.813	1.011	—	0.050 (10)
P. denitrificans	1	0.475	1.466	0.08 (1)	0.08 (1)
	2	0.472	1.466	0.07 (1)	0.08 (1)
	3	2.343	1.466	—	0.08 (1)

*In analysis 1, the spectra were analyzed with the constraint that $A_{o_1}^u = A_{o_1}^{CO}$. For analysis 2 the amplitude of component 1 was allowed to vary for the two states of the enzyme. In analysis 3, the component at 450 nm is not included in the model of the $a^{2+}a_3^{2+}$ state, and therefore, no value of $A_{o_1}^u$ is given. $^{\#}\chi_u^2$ and χ_{CO}^2 are the sums of squared residuals for the $a^{2+}a_3^{2+}$ *and* $a^{2+}a_3^{2+}$·CO states of the beef heart or *P. denitrificans* enzyme, respectively. $A_{o_1}^u$ and $A_{o_1}^{CO}$ are the amplitudes of the component at 22,130 cm^{-1} (component 1 in Fig. 8) for the $a^{2+}a_3^{2+}$ *and* $a^{2+}a_3^{2+}$·CO states of the enzyme. Uncertainty in the last digit of each amplitude, given in parentheses, is the sample standard deviation of nine independent measures.

absorption spectrum of cytochrome *c* oxidase in frozen solutions at cryogenic temperatures.

The spectrum of the mixed-valence $a^{2+}a_3^{3+}$·$HCOO^-$ form of cytochrome *c* oxidase at 10 K, as shown in Fig. 5, confirms that at least two absorption components underlie the absorption spectrum of cytochrome *a* in the Fe^{2+} oxidation state when the heme *A* group of cytochrome a_3 is bound to ligand. Since the second derivative spectrum selectively enhances narrow features of the absorption spectrum, it could have been argued that the feature at 450 nm in the second derivative spectrum of cytochrome *c* oxidase at room temperature represented a very narrow but insignificant detail of the spectrum. Observation of the 450-nm component in the direct absorption spectrum at 10 K rules out the possibility that the 450-nm feature is simply a computational artifact and affirms the sensitivity of second derivative spectroscopy to subtle changes in curvature due to separate, overlapping, unresolved bands.

The doublet features at 440 and 450 nm observed for ligand-bound states of cytochrome *c* oxidase were resolved also in the second derivative absorption spectra for the unliganded $a^{2+}a_3^{2+}$ form of the enzyme at cryogenic temperatures but not at room temperature (cf., Fig. 6). One possible mechanism for the observation of the doublet features for the unliganded state of cytochrome *c* oxidase at only cryogenic temperatures is a conformational equilibrium of the enzyme, which is temperature sensitive with the conformation absorbing maximally at 450 nm accumulating to an increasingly greater extent at lower and lower temperatures. Such a hypothesis would require that the conformational equilibrium exists at temperatures approaching the glass transition of the solvent as in fluid solution. If conformational adjustments are possible at such low temperatures, this model then predicts that the relative integrated absorption intensities of components underlying the absorption spectrum should change with temperature, contrary to experimental results. Moreover, no change in the integrated absorption intensities of the absorption components was necessary to account for the increased intensity of the feature at 450 nm at low temperatures, as shown in Fig. 6 and Table 2. The effect of temperature on absorption component linewidth (Fig. 7) explains the alterations of the direct and second derivative spectrum with changes in temperature without invoking an underlying conformational equilibrium of the protein.

Effect of ligand binding on the absorption spectrum of cytochrome *a*

In contrast to previously reported observations of second derivative spectra of the enzyme at room temperature (Sherman et al., 1991), the results from analysis of direct and second derivative absorption spectra of cytochrome *c* oxidase presented here indicate that the doublet features underlying the spectrum of cytochrome *a* are present in both ligand-bound and unliganded states of the enzyme. As demonstrated by the analysis described in Figs. 8 and 9, the absorption spectrum of cytochrome *a* is insensitive to the nature of the ligand at cytochrome a_3. The fit to the measured spectra improved dramatically when the 450-nm component was incorporated into the model of the spectrum of the unliganded enzyme (compare analysis 1 or 2 with analysis 3 in Table 2). Furthermore, varying the amplitude of the 450-nm component in response to changes in the ligand state of cytochrome a_3 did not significantly decrease the sum of squared absorption and second derivative residuals (cf., Tables 2 and 3). The apparent absence of the doublet features at 440 and 450 nm in the second derivative spectrum of the unliganded state of the enzyme at room temperature must, therefore, be ascribed to spectral overlap between the absorption spectrum of cytochrome a_3 and that of cytochrome *a*.

These results are in accord with the hypothesis that the heme group of cytochrome *a* behaves as an isolated chromophore and its spectral properties are not altered by ligand binding transitions in cytochrome a_3. The quantitative analysis of second derivative absorption spectra presented here is consistent with results of studies by others on the basis of the reduced-minus-oxidized absorption spectrum (Blair et al., 1982) and magnetic circular dichroism spectrum (Babcock et al., 1976) of cytochrome *a*, which show no evidence

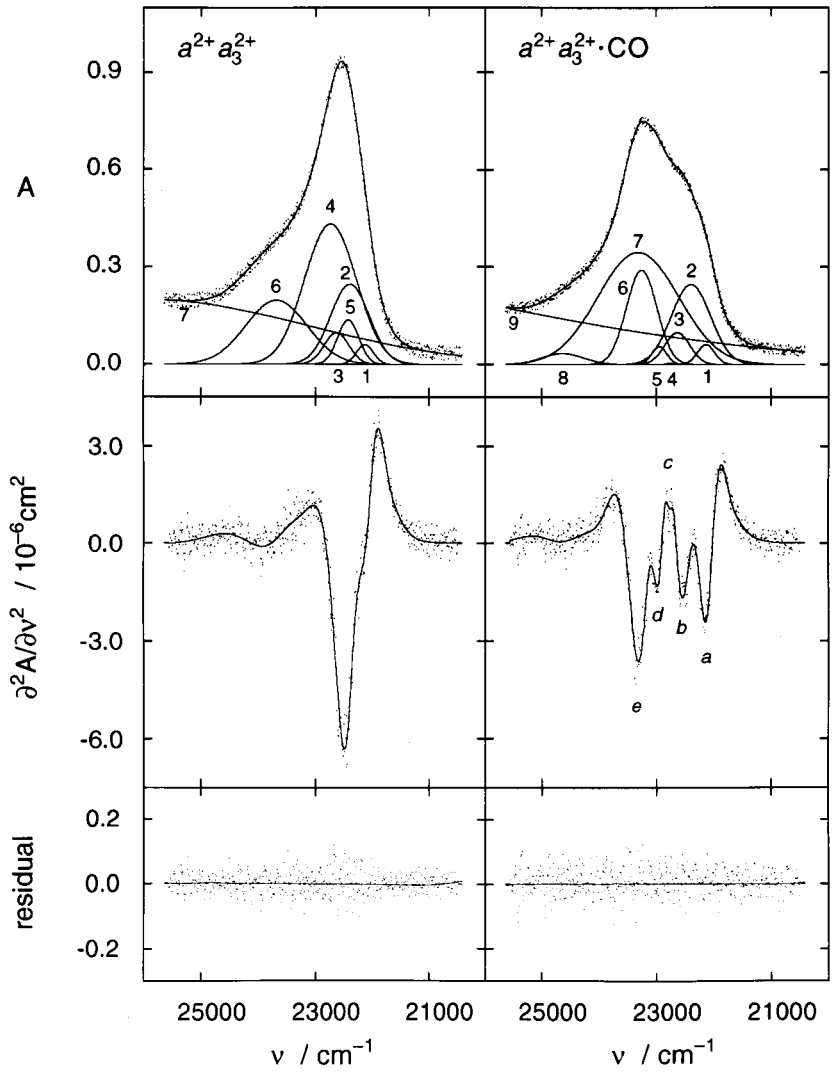

FIGURE 8 Analysis of the direct and second derivative absorption spectra of the $a^{2+}a_3^{2+}$ and $a^{2+}a_3^{2+}$·CO states of beef heart cytochrome *c* oxidase at 298 K. The spectra of the $a^{2+}a_3^{2+}$ state were modeled with seven components, and the spectra of the $a^{2+}a_3^{2+}$·CO state were modeled with nine components. Direct absorption spectra are shown in the top panels, second derivative spectra are shown in the middle panels, and the residuals for absorption data (*solid line*) and second derivative data (*points*) are shown in the bottom panels. In the analysis, components 1–3, which model features *a* and *b* at low energy in the second derivative spectrum of the $a^{2+}a_3^{2+}$·CO state were also included with equal intensity in the model of the spectrum of the $a^{2+}a_3^{2+}$ state of the enzyme. This analysis corresponds to analysis 1 of Table 2. The underlying assumption made in this analysis was that the absorption spectrum of cytochrome *a*, which gives rise to features *a* and *b* at low energy, is not perturbed by ligand binding at cytochrome a_3. In the analysis of the $a^{2+}a_3^{2+}$ state, components 4 and 5 model the additional intensity in the direct and second derivative absorption spectra that is not accounted for by components 1–3 assigned to the absorption of cytochrome *a*. Components 4 and 5 approximate the absorption of cytochrome a_3, which overlaps with the absorption of cytochrome *a* for this form of the enzyme. In the analysis of the $a^{2+}a_3^{2+}$·CO state, components 4–7 model features *c*-*e* present in the second derivative spectrum and, thus, approximate the absorption of a_3^{2+}·CO. For this region of the spectrum, there is a doublet feature at 430 nm (feature *e*, component 6 at 23,260 cm^{-1}) and 436 nm (feature *d*, component 5 at 22,950 cm^{-1}) due to a_3^{2+}·CO. Absorption data were recorded at 0.2-nm intervals and were transformed to be equally spaced in the wavenumber domain with Δx equal to 10 cm^{-1}. For the purpose of displaying the absorption data and model curve on one graph, scatter equal to approximately 2% of the absorption range was added to the absorption data as in Fig. 6. The spectral width of the Savitzky–Golay filter used in the calculation of second derivative spectra was 160 cm^{-1}.

that the spectroscopic properties of the heme group of cytochrome *a* are influenced through changes in the ligand and oxidation state of cytochrome a_3. Analysis of the second derivative and direct absorption spectra, as presented here, leads to the conclusion that, within experimental uncertainty, the structural changes associated with ligand binding (Sherman et al., 1991) and reduction at cytochrome a_3 and distal metal centers are not reflected in spectral features attributed to cytochrome *a* and detectable by second derivative absorption spectroscopy.

Molecular origin of the two-component spectrum of ferrocytochrome *a*

The absorption spectrum of the $a^{2+}a_3^{3+}$·$HCOO^-$ form of cytochrome *c* oxidase at 10 K, as shown in Fig. 5, provides

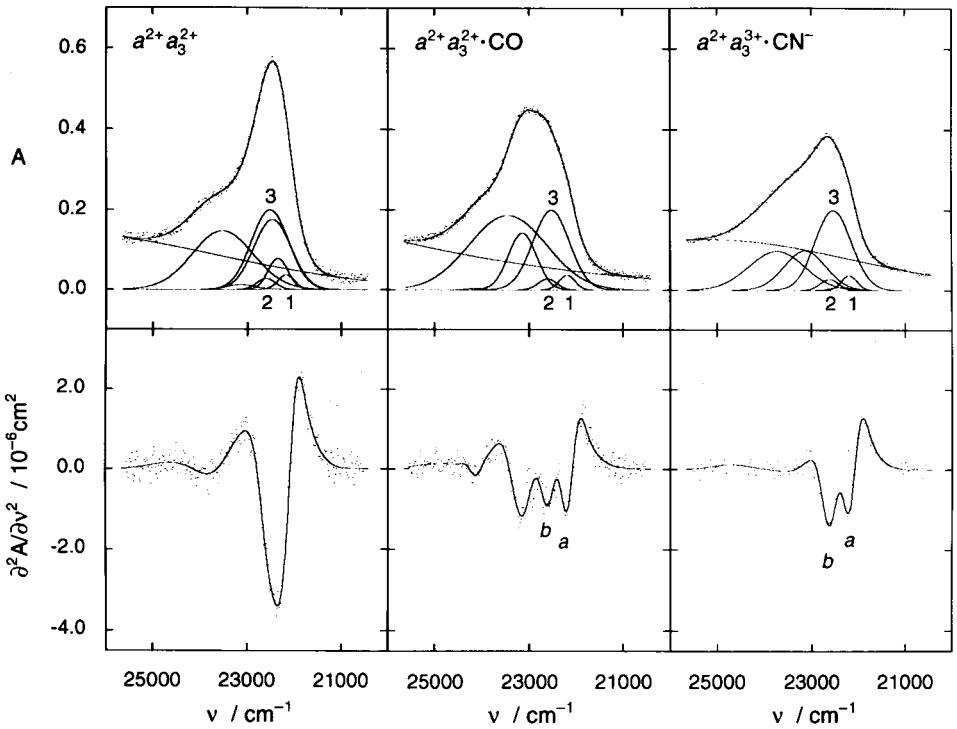

FIGURE 9 Analysis of the $a^{2+}a_3^{2+}$, $a^{2+}a_3^{2+}$·CO, and $a^{2+}a_3^{3+}$·CN^- states of *P. denitrificans* cytochrome *c* oxidase. Eight components model the spectrum of the unliganded $a^{2+}a_3^{2+}$ state, the $a^{2+}a_3^{2+}$·CO state, and the $a^{2+}a_3^{3+}$·CN^- state. The analysis shown here applies the constraint that the amplitude of the components that model the spectrum of cytochrome *a* (components 1–3) are, respectively, accorded equal intensity for each of the three states of the protein. This analysis corresponds to analysis 1 of Table 3. A parallel analysis in which the amplitude of the component at lowest energy (component 1) is allowed to vary for each of the three states of the enzyme did not result in a significantly better fit to the data (cf., analysis 2 of Table 3).

the clearest evidence for the two-component nature of the absorption spectrum of ferrocytochrome *a*. The two components have been inferred also on the basis of low-temperature difference spectra (Wilson and Gilmour, 1967; Wikström et al., 1976) and on the basis of room-temperature second derivative spectra (Copeland, 1991, 1993; Ishibe et al., 1991; Sherman et al., 1991; Lynch et al., 1992; Felsch et al., 1994). Since these two components are not dependent on the ligand and oxidation state of cytochrome a_3, as demonstrated in this investigation, they cannot be ascribed to transmission of protein structural changes from cytochrome a_3 to cytochrome *a*. Therefore, this observation suggests that the doublet components are intrinsic to the heme *A* chromophore and are probably due simply to lifting of the degeneracy of the *x*- and *y*-polarized components of the Soret B transition through symmetry lowering. This conclusion finds support in the results of magnetic circular dichroism studies of model heme *A* complexes.

The magnetic circular dichroism spectrum of the ferrous *bis*(1-methylimidazole)-heme *A* complex, a model compound for cytochrome *a*, reveals Faraday B terms at 570 and 595 nm of opposite signs, indicating a splitting of 740 cm^{-1} for *x*- and *y*-polarized transitions of the Q_0 band as a consequence of lowered symmetry (Carter and Palmer, 1982). A similar magnetic circular dichroism spectrum is observed for bacteriochlorophyll *a* (Sutherland and Olson, 1981). The symmetry point group of bacteriochlorophyll *a* is D_{2h} or lower as a consequence of hydrogenation of the two pyrrole rings, which are positioned diametrically across from each other in the porphyrin molecule. The formyl and vinyl substituents of heme *A* along one axis of the porphyrin macrocycle could similarly account for the lowered sym-

TABLE 3 Quantitative analysis of second derivative spectra of $a^{2+}a_3^{2+}$, $a^{2+}a_3^{2+}$·CO, and $a^{2+}a_3^{3+}$·CN^- states of cytochrome *c* oxidase from *P. denitrificans* and beef heart mitochondria

Enzyme	Analysis*	$\chi^{2\#}_{u}$	χ^2_{CO}	$\chi^2_{CN^-}$	A^{u}_{o1}	A^{CO}_{o1}	$A^{CN^-}_{o1}$
P. denitrificans	1	0.323	1.091	0.823	0.037 (4)	0.037 (4)	0.037 (4)
	2	0.322	1.087	0.825	0.032 (6)	0.038 (4)	0.036 (4)
Beef heart	1	0.159	0.436	0.556	0.046 (4)	0.046 (4)	0.046 (4)
	2	0.158	0.428	0.550	0.052 (5)	0.049 (5)	0.043 (5)

*In analysis 1, the spectra of the three states of cytochrome *c* oxidase were analyzed with the constraint that $A^{u}_{o1} = A^{CO}_{o1} = A^{CN^-}_{o1}$. For analysis 2 the amplitude of component 1 was allowed to vary for each state of the enzyme. It is seen that there is no statistically significant difference in the results for analyses 1 and 2 for both the *P. denitrificans* and the beef heart enzymes.

#χ^2_u, χ^2_{CO}, and $\chi^2_{CN^-}$ are the sums of squared residuals for the $a^{2+}a_3^{2+}$, $a^{2+}a_3^{2+}$·CO, and $a^{2+}a_3^{3+}$·CN^- states of the *P. denitrificans* and beef heart enzymes. A^{u}_{o1}, A^{CO}_{o1}, and $A^{CN^-}_{o1}$ are the amplitudes of component 1 in Fig. 9 for the $a^{2+}a_3^{2+}$, $a^{2+}a_3^{2+}$·CO, and $a^{2+}a_3^{3+}$·CN^- states of the *P. denitrificans* enzyme. Uncertainty in the last digit of each amplitude, given in parentheses, is the sample standard deviation of nine independent measures.

metry of hexa-coordinated heme *A* (Carter and Palmer, 1982). These correlated findings and the observation that cytochrome *a* exhibits doublet features support the notion that asymmetry intrinisic to the heme *A* molecule is responsible for the doublet second derivative features rather than a special interaction with the protein environment.

APPENDIX: THE SAVITZKY–GOLAY FILTER

The values defining the Savitzky–Golay filter for calculation of second derivative spectra by the simplified least-squares method are obtained in the following manner. To calculate the second derivative of the absorption spectrum, N data points $\{(x_i, y_i)\}$ are selected and the absorption values are modeled by a fourth-order (quartic) polynomial, the general form of which is given by

$$\tilde{y}_i = a_4 x_i^4 + a_3 x_i^3 + a_2 x_i^2 + a_1 x_i + a_0\,, \tag{A1}$$

where $\tilde{y}_i$ is the approximation of the ith absorption value y_i. The second derivative of $\tilde{y}_i$ calculated at x_0 is the approximated value of the second derivative of the data. To simplify the arithmetic and to be able to apply the method to a general set of data, the domain particular to the data is transformed to the domain of i so that $x_i = i$. The values of i range from $-(N-1)/2$ to $(N-1)/2$, where N is an odd integer ≥ 5. A scaling factor of Δx^{-2} is introduced as a consequence of this transformation, where Δx is the interval measured between x_i and $x_{(i+1)}$. After transforming the domain in this manner, the second derivative of the data is approximated by Eq. A2, where $\tilde{y}''_0$ is the approximate value of the second derivative of the data at $i = 0$,

$$\tilde{y}''_0 = \Delta x^{-2} \cdot 2 \cdot a_2\,. \tag{A2}$$

To evaluate Eq. A2, the value of the coefficient a_2 must be determined. The values of each of the coefficients of Eq. A1 $\{a_j\}$ are those that minimize the sum of squared residuals χ^2 described by

$$\chi^2 = \sum_{i=-(N-1)/2}^{(N-1)/2} (y_i - \tilde{y}_i)^2\,. \tag{A3}$$

The simplified least-squares method, as used in this investigation, refers to the minimization of the squared residuals in Eq. A3 (Savitzky and Golay, 1964) .

Minimization of the squared residuals is carried out by differentiating Eq. A3 with respect to each of the coefficients $\{a_j\}$ and setting each derivative equal to zero as described by

$$\frac{\partial \chi^2}{\partial a_j} = -2 \sum_i (y_i - \tilde{y}_i)\, x_i^j = 0, \tag{A4}$$

which can be rewritten as

$$\begin{bmatrix} \sum x_i^8 & 0 & \sum x_i^6 & 0 & \sum x_i^4 \\ 0 & \sum x_i^6 & 0 & \sum x_i^4 & 0 \\ \sum x_i^6 & 0 & \sum x_i^4 & 0 & \sum x_i^2 \\ 0 & \sum x_i^4 & 0 & \sum x_i^2 & 0 \\ \sum x_i^4 & 0 & \sum x_i^2 & 0 & N \end{bmatrix} \begin{bmatrix} a_4 \\ a_3 \\ a_2 \\ a_1 \\ a_0 \end{bmatrix} = \begin{bmatrix} \sum y_i x_i^4 \\ \sum y_i x_i^3 \\ \sum y_i x_i^2 \\ \sum y_i x_i^1 \\ \sum y_i x_i^0 \end{bmatrix}. \tag{A5}$$

The pattern of zeroes in the matrix of Eq. A5 results from the fact that the value of x_i acquires negative and positive values ranging from $-(N-1)/2$ to $(N-1)/2$. Because of the asymmetry in x_i, the summation over x_i^p with an odd value of p is zero.

Eq. A5 can be solved by matrix inversion to give the values of the coefficients $\{a_j\}$ in terms of the data values $\{y_i\}$. Eq. A2 can then be expressed as the weighted sum of the data values according to

$$\tilde{y}''_0 = \Delta x^{-2} \cdot 2 \cdot a_2 = \Delta x^{-2} \sum_i w_i y_i\,, \tag{A6}$$

where w_i is the ith value of the Savitzky–Golay filter.

Matrix inversion of the 5×5 matrix in Eq. A5 is cumbersome; therefore, a simpler example of the derivation of the values of $\{w_i\}$ is provided below. In this example, in place of the quartic polynomial of Eq. A1, the data values are modeled using the quadratic polynomial given in

$$\tilde{y}_i = a_2 x_i^2 + a_1 x_i + a_0. \tag{A7}$$

The second derivative of the data is still approximated by Eq. A2. Proceeding as above to determine the value of the coefficient a_2 leads to

$$\begin{bmatrix} \sum x_i^4 & 0 & \sum x_i^2 \\ 0 & \sum x_i^2 & 0 \\ \sum x_i^2 & 0 & N \end{bmatrix} \begin{bmatrix} a_2 \\ a_1 \\ a_0 \end{bmatrix} = \begin{bmatrix} \sum y_i x_i^2 \\ \sum y_i x_i^1 \\ \sum y_i x_i^0 \end{bmatrix}, \tag{A8}$$

which is analogous to Eq. A5. The inverse of the 3×3 matrix of Eq. A8 is given by

$$\begin{bmatrix} \sum x_i^4 & 0 & \sum x_i^2 \\ 0 & \sum x_i^2 & 0 \\ \sum x_i^2 & 0 & N \end{bmatrix}^{-1} = \begin{bmatrix} N/\Delta & 0 & -\sum x_i^2/\Delta \\ 0 & 1/\sum x_i^2 & 0 \\ -\sum x_i^2/\Delta & 0 & \sum x_i^4/\Delta \end{bmatrix}, \tag{A9}$$

where

$$\Delta = N \sum x_i^4 - (\sum x_i^2)^2\,.$$

TABLE A1 Sample calculations of $\{w_i\}$ for Savitzky–Golay filters derived from least-squares minimization of a quadratic model of N data points*

N	$\Sigma\, x_i^2$	$\Sigma\, x_i^4$	Δ	$\{w_i\}$
3	2	2	2	{1/2, −2/2, 1/2}
5	10	34	70	{2/7, −1/7, −2/7, −1/7, 2/7}
7	28	196	588	{5/42, 0, −3/42, −4/42, −3/42, 0, 5/42}
9	60	708	2772	{28/462, 7/462, −8/462, −17/462, −20/462, −17/462, −8/462, 7/462, 28/462}

*For $N = 3$, $\{x_i\} = \{-1, 0, 1\}$, for $N = 5$, $\{x_i\} = \{-2, -1, 0, 1, 2\}$, for $N = 7$, $\{x_i\} = \{-3, -2, -1, 0, 1, 2, 3\}$, and for $N = 9$, $\{x_i\} = \{-4, -3, -2, -1, 0, 1, 2, 3, 4\}$. Δ is evaluated as $N \Sigma\, x_i^4 - (\Sigma\, x_i^2)^2$, which is the denominator of Eq. A12. The ith value of the Savitzky–Golay filter w_i is represented by the fraction obtained after dividing the numerator and denominator of Eq. A12 by a common integer factor. This factor was 1 for $N = 3$, 10 for $N = 5$, 14 for $N = 7$, and 6 for $N = 9$.

TABLE A2 Savitzky–Golay filters derived from least-squares minimization of a quartic model of *N* data points*

	$N = 25$	$N = 23$	$N = 21$	$N = 19$	$N = 17$	$N = 15$	$N = 13$	$N = 11$	$N = 9$	$N = 7$	$N = 5$
$\Delta \cdot w_{\pm 12}$	−429,594										
$\Delta \cdot w_{\pm 11}$	31,119	−346,731									
$\Delta \cdot w_{\pm 10}$	298,155	61,845	−37,791								
$\Delta \cdot w_{\pm 9}$	413,409	281,979	11,628	−96,084							
$\Delta \cdot w_{\pm 8}$	414,786	358,530	35,802	45,084	−121,524						
$\Delta \cdot w_{\pm 7}$	336,201	331,635	41,412	105,444	82,251	−93,093					
$\Delta \cdot w_{\pm 6}$	207,579	236,709	34,353	109,071	153,387	88,803	−72,963				
$\Delta \cdot w_{\pm 5}$	54,855	104,445	19,734	76,830	137,085	133,485	98,010	−10,530			
$\Delta \cdot w_{\pm 4}$	−100,026	−39,186	1,878	26,376	71,592	95,568	115,632	20,358	−4,158		
$\Delta \cdot w_{\pm 3}$	−239,109	172,935	−15,678	−27,846	−11,799	19,737	53,262	17,082	12,243	−117	
$\Delta \cdot w_{\pm 2}$	−348,429	−280,275	−30,183	−74,601	−88,749	−59,253	−32,043	117	4,983	603	−3
$\Delta \cdot w_{\pm 1}$	−418,011	−349,401	−39,672	−105,864	−141,873	−116,577	−99,528	−15,912	−6,963	−171	48
$\Delta \cdot w_0$	−441,870	−373,230	−42,966	−116,820	−160,740	−137,340	−124,740	−22,230	−12,210	−630	−90
Δ	51,505,740	33,745,140	2,941,884	5,883,768	5,744,232	3,325,608	1,925,352	200,772	56,628	1,188	36

*Adapted from Table 7 of Savitzky and Golay (1964) with corrections. To obtain the *i*th value of the Savitzky–Golay filter, divide $\Delta \cdot w_i$ by Δ.

With the use of the inverse matrix, the coefficient a_2 can be evaluated as

$$a_2 = \frac{\sum (Nx_i^2 - \sum x_i^2)y_i}{N \sum x_i^4 - (\sum x_i^2)^2}. \quad \text{(A10)}$$

By substituting Eq. A10 into Eq. A6, the second derivative of the data is evaluated as

$$\tilde{y}_0'' = \Delta x^{-2}\left[2\frac{\sum (Nx_i^2 - \sum x_i^2)y_i}{N \sum x_i^4 - (\sum x_i^2)^2}\right] = \Delta x^{-2} \sum_i w_i y_i. \quad \text{(A11)}$$

Inspection of Eq. A11 shows that the values of the Savitzky–Golay filter $\{w_i\}$ are now expressed in terms of the values of $\{x_i\}$, which are constant for a given filter of N points. Thus, the *i*th value of the Savitzky–Golay filter can be calculated according to

$$w_i = 2\frac{Nx_i^2 - \sum x_i^2}{N \sum x_i^4 - (\sum x_i^2)^2}. \quad \text{(A12)}$$

As examples of the application of Eq. A12, the values of $\{w_i\}$ for Savitzky–Golay filters with $N = 5$, $N = 7$, and $N = 9$ are given in Table A1. The values of $\{w_i\}$ obtained in Table A1 are exactly the same as values reported in the literature (Savitzky and Golay, 1964; Steiner et al., 1972).

More lengthy arithmetic is required to obtain the values of $\{w_i\}$ for Savitzky–Golay filters that make use of a quartic model, but the process is analogous to the simple example given above, which applies a quadratic model. The advantage gained by the quartic model is an improvement in accuracy of the second derivative calculation because the additional terms in the quartic polynomial allow the data to be approximated more closely. The Savitzky–Golay filters derived from a quartic model of N data points are provided in Table A2. Tables similar to that of Table A2 can be found in the literature (Savitzky and Golay, 1964; Steiner et al., 1972).

We thank Dr. Melissa Calhoun for assistance with the 77 K cryospectrophotometer in the laboratory of Professor Robert Gennis and Dr. Donald Lamb for assistance with the variable-temperature cryospectrophotometer in the laboratory of Professor Hans Frauenfelder. Paul Goudreau participated in early stages of developing the purification procedure for the P. denitrificans cytochrome *c* oxidase. We acknowledge helpful conversations with Dr. Vukica Šrajer and the late Professor Howard S. Tager. M.P.H. was supported by a National Science Foundation predoctoral fellowship and by a training grant of the National Institutes of Health (GM07183). M.W.M. was supported by a grant of the National Institutes of Health (GM21900), and R.A.C was supported by an Established Investigatorship of the American Heart Association, a Syntex Scholars Award, a Shannon Award of the National Institutes of Health, and by the Martin D. and Virginia S. Kamen Sustaining Fund for Junior Faculty at The University of Chicago.

REFERENCES

Antholine, W. E., D. H. W. Kastrau, G. C. M. Steffens, G. Buse, W. G. Zumft, and P. M. H. Kroneck. 1992. A comparative EPR investigation of the multicopper protein nitrous-oxide reductase and cytochrome *c* oxidase. *Eur. J. Biochem.* 209:875–881.

Babcock, G. T., L. E. Vickery, and G. Palmer. 1976. Electronic state of heme in cytochrome oxidase. I. Magnetic circular dichroism of the isolated heme and its derivatives. *J. Biol. Chem.* 251:7907–7919.

Babcock, G. T., and M. Wikström. 1992. Oxygen activation and the conservation of energy in cell respiration. *Nature.* 356:301–309.

Blackburn, N. J., M. E. Barr, W. H. Woodruff, J. van der Oost, and S. de Vries. 1994. Metal–metal bonding in biology: EXAFS evidence for a 2.5 Å copper–copper bond in the Cu_A center of cytochrome oxidase. *Biochemistry.* 33:10401–10407.

Blair, D. F., D. F. Bocian, G. T. Babcock, and S. I. Chan. 1982. Evidence for modulation of the heme absorptions of cytochrome *c* oxidase by metal–metal interactions. *Biochemistry.* 21:6928–6935.

Bonfiglioli, G., and P. Brovetto. 1964. Principles of self-modulating derivative optical spectrophotometers. *Appl. Optics.* 3:1417–1424.

Cahill, J. E. 1979. Derivative spectroscopy: understanding its application. *Am. Lab.* 11:79–85.

Cahill, J. E., and F. G. Padera. 1980. Derivative analysis of uv/visible spectra. *Am. Lab.* 12:101–112.

Cameron, D. G., and D. J. Moffat. 1984. Deconvolution, derivation and smoothing of spectra using Fourier transforms. *J. Test. Eval.* 12:78–85.

Cameron, D. G., and D. J. Moffat. 1987. A generalized approach to derivative spectroscopy. *Appl. Spectrosc.* 41:539–544.

Carter, K., and G. Palmer. 1982. Models of the two heme centers in cytochrome oxidase. Optical properties of cytochrome *a* and a_3. *J. Biol. Chem.* 257:13507–13514.

Copeland, R. A. 1991. Conformational switching at cytochrome *a* during steady-state turnover of cytochrome *c* oxidase. *Proc. Natl. Acad. Sci. USA.* 88:7281–7283.

Copeland, R. A. 1993. Long-distance cofactor interactions in terminal oxidases studied by second-derivative absorption spectroscopy. *J. Bioenerg. Biomem.* 24:93–102.

DeVault, D. 1971. Energy transduction in electron transport. *Biochim. Biophys. Acta.* 226:193–199.

DeVault, D. 1976. Theory of iron-sulfur center N-2 oxidation and reduction by ATP. *J. Theor. Biol.* 62:115–139.

Felsch, J. S., M. P. Horvath, S. Gursky, M. R. Hobaugh, P. N. Goudreau, J. A. Fee, W. T. Morgan, S. J. Admiraal, M. Ikedo-Saito, T. Fujiwara, Y.

Fukumori, Y. Yamanaka, and R. A. Copeland. 1994. Probing protein-cofactor interactions in the terminal oxidases by second-derivative spectroscopy: study of bacterial enzymes with cofactor substitutions and heme *A* model compounds. *Protein Sci.* 3:2097–2103.

Green, G. L., and T. C. O'Haver. 1974. Derivative luminescence spectrometry. *Anal. Chem.* 46:2191–2196.

Hartzell, C. R., and H. Beinert. 1974. Components of cytochrome *c* oxidase detectable by EPR spectroscopy. *Biochim. Biophys. Acta.* 368:318–338.

Hartzell, C. R., H. Beinert, B. F. van Gelder, and T. E. King. 1978. Preparation of cytochrome oxidase from beef heart. *Methods Enzymol.* 53:54–66.

Horvath, M. P. 1994. Electron transfer and metal–metal interactions in cytochrome oxidase. Ph.D. thesis, The University of Chicago, Chicago, IL.

Ishibe, N., S. R. Lynch, and R. A. Copeland. 1991. The pH dependence of cytchrome *a* conformation in cytochrome *c* oxidase. *J. Biol. Chem.* 266:23916–23920.

Jencks, W. P. 1980. The utilization of binding energy in coupled vectorial processes. *Adv. Enzymol.* 51:75–106.

Kaschny, P., and F. M. Goñi. 1992. The components of merocyanine-540 absorbance spectra in aqueous, micellar and bilayer environments. *Eur. J. Biochem.* 207:1085–1091.

Kauppinen, J. K., D. J. Moffat, D. G. Cameron, and H. H. Mantsch. 1981a. Noise in Fourier self-deconvolution. *Appl. Opt.* 20:1866–1879.

Kauppinen, J. K., D. J. Moffat, H. H. Mantsch, and D. G. Cameron. 1981b. Fourier transforms in the computation of self-deconvoluted and first order derivative spectra of overlapped band contours. *Anal. Chem.* 53:1454–1457.

Lynch, S. R., D. Sherman, and R. A. Copeland. 1992. Cytochrome *c* binding affects the conformation of cytochrome *a* in cytochrome oxidase. *J. Biol. Chem.* 267:298–302.

Mantsch, H. H., D. J. Moffat, and H. L. Casal. 1988. Fourier transform methods for spectral resolution enhancement. *J. Mol. Struct.* 173: 285–298.

Marquardt, D. W. 1963. An algorithm for least-squares estimation of nonlinear parameters. *J. Soc. Indust. Appl. Math.* 11:431–441.

Martin, A. E. 1957. Difference and derivative spectra. *Nature.* 180: 231–233.

Nicholls, P. 1976. The effect of formate on cytochrome aa_3 and on electron transport in the intact respiratory chain. *Biochim. Biophys. Acta.* 430: 13–29.

O'Haver, T. C., and T. Begley. 1981. Signal-to-noise ratio in higher order derivative spectrometry. *Anal. Chem.* 53:1876–1878.

Pleshko, N., A. Boskey, and R. Mendelsohn. 1991. Novel infrared spectroscopic method for the determination of crystallinity of hydroxyapatite minerals. *Biophys. J.* 60:786–793.

Rasmussen, D. H., and A. P. MacKenzie. 1971. The glass transition in amorphous water. Application of the measurements to problems arising in cryobiology. *J. Phys. Chem.* 75:967–973.

Saraste, M. 1990. Structural features of cytochrome oxidase. *Quart. Rev. Biophys.* 23:331–366.

Savitzky, A., and M. J. E. Golay. 1964. Smoothing and differentiation of data by simplified least squares procedures. *Anal. Chem.* 36:1627–1639.

Sherman, D., S. Kotake, N. Ishibe, and R. A. Copeland. 1991. Resolution of the electronic transitions of cytochrome *c* oxidase: evidence for two conformational states of ferrous cytochrome *a. Proc. Natl. Acad. Sci. USA.* 88:4265–4269.

Steiner, J., Y. Termonia, and J. Deltour. 1972. Comments on smoothing and differentiation of data by simplified least square procedure. *Anal. Chem.* 44:1906–1909.

Sutherland, J. C., and J. M. Olson. 1981. Magnetic circular dichroism of bacteriochlorophyll *a* in solution and in a protein. *Photochem. Photobiol.* 33:379–384.

Tanford, C. 1983. Mechanism of free energy coupling in active transport. *Annu. Rev. Biochem.* 52:379–409.

Torres, J., and E. Padrós. 1993. The secondary structure of bacteriorhodopsin in organic solution. *FEBS Lett.* 318:77–79.

Tsukihara, T., H. Aoyama, E. Yamashita, T. Tamizaki, H. Yamaguchi, K. Shinzawma-Itoh, R. Nakashima, R. Yaomo, and S. Yoshikawa. 1995. Structures of metal sites of oxidized bovine heart cytochrome *c* oxidase at 2.8 Å. *Science.* 269:1069–1074.

van Wachenfeldt, C., S. de Vries, and J. van der Oost. 1994. The Cu_A site of the aa_3-type oxidase of *Bacillus subtilis* is a mixed-valence binuclear copper center. *FEBS Lett.* 340:109–113.

Vanneste, W. H. 1966. The stoichiometry and absorption spectra of components *a* and a_3 in cytochrome *c* oxidase. *Biochemistry.* 5:838–848.

Wikström, M., and K. Krab. 1979. Proton-pumping cytochrome *c* oxidase. *Biochim. Biophys. Acta.* 549:177–222.

Wikström, M. K. F. 1977. Proton pump coupled to cytochrome *c* oxidase in mitochondria. *Nature.* 266:271–273.

Wikström, M. K. F., J. Harmon, W. J. Ingledew, and B. Chance. 1976. A re-evaluation of the spectral, potentiometric and energy-linked properties of cytochrome *c* oxidase in mitochondria. *FEBS Lett.* 65:259–277.

Williams, D. T., and R. N. J. Hager. 1970. The derivative spectrometer. *Appl. Opt.* 9:1597–1605.

Wilson, D. F., and M. V. Gilmour. 1967. The low-temperature spectral properties of mammalian cytochrome oxidase. I. The enzyme in intact rat-liver mitochondria. *Biochim. Biophys. Acta.* 143:52–61.

Yannas, I. 1968. Vitrification temperature of water. *Science.* 160:298–299.